


12-2013

Tin Sensitization For Electroless Plating

Xingfei Wei

University of Arkansas, Fayetteville

Follow this and additional works at: <http://scholarworks.uark.edu/etd>

 Part of the [Organic Chemistry Commons](#), and the [Process Control and Systems Commons](#)

Recommended Citation

Wei, Xingfei, "Tin Sensitization For Electroless Plating" (2013). *Theses and Dissertations*. 976.
<http://scholarworks.uark.edu/etd/976>

This Thesis is brought to you for free and open access by ScholarWorks@UARK. It has been accepted for inclusion in Theses and Dissertations by an authorized administrator of ScholarWorks@UARK. For more information, please contact scholar@uark.edu, ccmiddle@uark.edu.

Tin Sensitization For Electroless Plating

Tin Sensitization For Electroless Plating

A thesis submitted in partial fulfillment
of the requirements for the degree of
Master of Science in Chemical Engineering

By

Xingfei Wei
Zhejiang University
Bachelor of Energy & Environment Systems Engineering, 2010

December 2013
University of Arkansas

This thesis is approved for recommendation to the Graduate Council.

Dr. Donald Keith Roper
Thesis Director

Dr. Rick Ulrich
Committee Member

Dr. Jingyi Chen
Committee Member

ABSTRACT

The tin sensitization process has been used in electroless plating since 1940s Brenner and Riddell developed the electroless plating for surface metallization method. It was found to be an interesting topic to study tin sensitization for chemically controlling metal deposition on different substrates, because the tin sensitization process had critical effects on the electroless plated metal thin films. Nowadays electroless plating metal deposition is still an important method for depositing metals. It has a few advantages over the vapor deposition and electrodeposition method, such as work in an ambient condition, on nonconductive substrates, and without extra power input. Applying electroless plating our lab has successfully fabricated ordered array of gold nanostructures, for example Dr. Blake fabricated gold nano rings by top-down electron-beam lithography, and Dr. Ahn fabricated hexagonal gold nano particles by bottom-up silica sphere self-assembly. Dr. Jang studied the silver catalytic particle formation and gold thin film dynamically formation in detail. However, the tin sensitization process has not be studied yet. Therefore, in this master's thesis the tin sensitization for electroless plating was researched.

In Chapter I an introduction was given for the tin sensitization process and the electroless plating method. In Chapter II the tin sensitization process for electroless plating was reviewed. In Chapter III a rapid, straightforward, spectrophotometric method, based on the redox reaction of tin(II) with a mixture of N-bromosuccinimide (NBS) and 3,3',5,5'-tetramethylbenzidine dihydrochloride (TMB-d) was developed for determining low concentrations of tin(II). In Chapter IV the spectrophotometric method developed in Chapter II was developed for quantitative measurement of stannous (tin(II)) concentrations on ceramic substrates. Effects of reagent concentration, exposure time, substrate physicochemistry, and post-exposure conditions on surface tin(II) content were evaluated. Aqueous immersion post-reaction doubled tin(II) surface concentration compared to drying in nitrogen before a two-minute air exposure. In

Chapter V the 2D hexagonal arrays of gold nano rings were fabricated by coupling EBL and electroless plating. The future work of applying the results in this thesis was proposed in Chapter VI. Two directions were suggested, uniform metal deposition that could be comparable to vacuum deposition methods and fabricating ordered array of metal nanostructures.

ACKNOWLEDGEMENTS

Special thanks are due to the Department of Chemical Engineering of the University of Arkansas for all the support with the study and research. Thank Dr. Roper for advising me in experiment and writing scientific articles. Without Dr. Roper's advising and help this work would not have been accomplished. Thank Prof. Ken Vickers for providing valuable advice. Thank Dr. Gyoung Gug Jang for his initial guide in the research. Thank Dr. Phillip Blake for his supervision on the research. Thank Dr. Milana Oleksandrivna Lisunova for her supervision in experiment and help with the thesis. Also thank all the group members for their help and discussions in the experiment. Jeremy, Greg, Drew, Vinith and Keith, thank you all for your help in the experiment setting up and results discussion. It was a great pleasure to work with you all. Finally, I thank my parents and friends for their supporting.

Also, special thanks go out to the faculty and staff at the University of Arkansas and in the Department of Chemical Engineering for their commitment to the University and to the students.

TABLE OF CONTENTS

I. INTRODUCTION	1
A. REFERENCES.....	3
II. TIN SENSITIZATION REVIEW	5
B. INTRODUCTION.....	5
C. CHARACTERISTICS OF TIN SENSITIZED SURFACES.....	6
Chemical composition of the tin.....	6
Contact angle measurement.....	7
Catalytic sites.....	9
Metal deposition island morphology	11
D. CONDITIONS TO PROCEED TIN SENSITIZATION.....	12
Aging solution	12
Substrates.....	13
E. TRIFLUOROACETIC ACID (TFA) IN TIN SENSITIZATION SOLUTION.....	15
F. PHOTO SELECTIVE METAL DEPOSITION (PSMD)	16
Idea development.....	16
Mechanism discuss	17
G. SINGLE-STEP TINSENSITIZATION	19
Method development and comparison with two-step system.....	19
Accelerator.....	21
Electrochemical method study.....	21
H. TIN SENSITIZATION MECHANISM DEVELOPMENT.....	22
Conventional two-step system.....	22

Single-step catalyzing system.....	26
I. APPLICATION OF TIN SENSITIZATION	27
J. CONCLUSION	28
K. REFERENCES.....	30
III. SPECTROPHOTOMETRIC METHOD FOR ANALYZING TIN(II) BY REDOX REACTION USING 3,3',5,5'-TETRAMETHYLBENZIDINE DIHYDROCHLORIDE AND N-BROMOSUCCINIMIDE	34
A. INTRODUCTION.....	34
B. EXPERIMENTAL METHOD.....	39
Apparatus.....	39
Reagents.....	40
Procedure.....	40
C. RESULTS AND DISCUSSION	42
Mechanism.....	42
Optimum detection condition	45
Evaluation of Method	50
D. CONCLUSIONS	52
E. REFERENCES.....	52
IV. TIN(II) CONCENTRATION ON TIN SENSITIZED SODA LIME GLASS SUBSTRATES	55
A. INTRODUCTION.....	55
B. EXPERIMENTAL METHOD.....	56
Materials	56

Procedure.....	57
C. RESULTS AND DISCUSSION	59
Sensitization time effect	59
Tin solution concentration effect.....	61
Hydrochloric acid (HCl) and substrates difference	62
Post exposure of the tin sensitized substrates	64
Effect on gold nucleation at the initial stage of electroless gold plating.....	65
D. CONCLUSIONS	69
E. REFERENCES.....	70
V. ELECTROLESS GOLD PLATING FOR 2D HEXAGONAL ARRAYS OF NANO RINGS AND 3D NANOSTRUCTURES GROWTH.....	72
A. INTRODUCTION.....	72
B. METHODS.....	74
C. RESULTS AND DISCUSSION	76
Gold film, ordered array of gold structures and top layer of gold film on the tape.....	76
Growing 3D gold nanostructures based on the 2D gold nano rings	77
D. CONCLUSIONS	84
E. REFERENCES.....	85
VI. CONCLUSION	87
VII. FUTURE WORK.....	88

I. INTRODUCTION

Fabrication of gold (Au) thin film is important in electronics [1], micro-electrochemical systems (MEMS) [2], Au-coated sensors [3], reactors [4], and catalysts [5]. A large number of methods can be used to make Au thin films on various substrates. Compared with sputtering, chemical vapor deposition (CVD), and physical vacuum deposition (PVD), electroless plating (EL) does not require expensive capital equipment or vacuum conditions. Compared with electro-deposition [6], conductive substrates and an external power supply are not needed for EL. Moreover, EL technology can be applied to unlimited substrate shapes; it is used to synthesize metal nanotubes on porous templates, for example [7].

Steps in electroless Au plating include substrate pretreatment, tin (Sn^{2+}) sensitization, silver (Ag) activation, and gold (Au) plating [8]. Controlling Au deposition time allows production of ultrathin uniform Au (111) films with enhanced features relative to sputtered Au films [9]. Random Au nanoparticle (NP) assemblies made from thermal transformation of Au film exhibited enhanced laser-to-heat transduction upon incident resonant irradiation at localized surface plasmon resonance (LSPR) frequency [10]. Regular arrays of Au NPs could be fabricated by depositing metal onto a pattern created by top-down electron (e)-beam lithography [11] or by bottom-up nanosphere self-assembly [12]. Using continuous flow to maintain a constant thermodynamic driving force and enhance mass transfer rates to the surface improved the Au film quality and enhanced its optical features [13]. Real-time transmission UV-vis (T-UV) spectroscopy was recently used to characterize disposition and dynamics of Ag disposition during and after Ag reduction onto the tin-sensitized surface during continuous flow [14]. These results suggest real-time T-UV spectroscopy of metal photoluminescence features could be used

to refine fluidic EL deposition of an epitaxial, uniform, atomically thin layer of Au by maintaining redox conditions (Lewis acid/base content, pH, and oxidation potential).

A number of improvements appear possible from continuous control of salt concentration and redox conditions during EL plating. Continuous-flow introduction of consecutive solutions could avoid exposure of the film to air. Only a metallic Ag thin film would form and an Au film should displace all the Ag film. Previously, X-ray photoelectron spectroscopy (XPS) of EL-deposited metal film showed both Ag metal and AgO_x remained in the more noble Au thin film [14]. The formation of AgO_x could be due to small quantities of dissolved oxygen in the solution, the high pH of the sodium gold sulfite solution [15] oxidizing the Ag NPs, or small size Ag NPs reducing Ag redox potential. An Ag- NH_3 - H_2O system similar to that found in the second step of EL plating was reported to have a pH-dependent redox potential [16]. Acid $\text{pH} < 7$ gave higher redox potential ($E > 0.7\text{V}$) than basic conditions ($E \sim 0.4\text{V}$) [16]. Silver reduction in the existing EL reduction uses ammoniac Ag titrated from a caustic preparation, without pH control. The pH-controlled reduction of Ag from acid-titrated di-amine complex at controlled pH appears more likely to result in a controlled reduction of Ag. Redox potential of silver clusters also appears size dependent. Smaller silver particles are reported to have more negative chemical potentials than larger ones. Silver atoms are strong electron donors with chemical potentials as negative as -1.8V [17].

Tin sensitization was the initial step for electroless plating, which deposited tin(II) on the substrates. Tin(II) will reduce palladium(II) and silver(I) to Pd^0 and Ag^0 , which were the catalytic sites for electroless plating. The surface morphology of the catalytic sites was related to the tin(II) concentration, while the catalytic sites on the surface controlled the metal deposition. The characteristics of tin sensitization were studied by different methods, such as tin(II)/tin(IV)

composition measurement, contact angle measurement, and catalytic sites characterization. The mechanism of tin sensitization was proposed and discussed in Chapter 2.

In this master's thesis the tin sensitization method was reviewed in Chapter 2. A spectrophotometric method was developed for determining tin(II) concentration in solution in Chapter 3. A study of this applied method for quantifying the tin(II) concentration on substrates at various conditions was summarized in Chapter 4. Finally, 2D gold nano rings were fabricated based on electron-beam-lithography (EBL) and 3D structure growth based on the 2D nano ring was tested in Chapter 5. Future work including electroless plating method improvement and application was proposed.

A. REFERENCES

- (1). Osaka, T.; Kodera, A.; Misato, T.; Homma, T.; Okinaka, Y. *J. Electrochem. Soc.*, Vol. 144, No. 10, October 1997.
- (2). Ashurst, W. R.; Carraro, C.; Maboudian, R. *IEEE TRANSACTIONS ON DEVICE AND MATERIALS RELIABILITY*, VOL. 3, NO. 4, DECEMBER 2003.
- (3). Ko, J. W.; Koo, H. C.; Kim, D. W.; et al. *Journal of The Electrochemical Society*, 157 (1) D46-D49 (2010).
- (4). Wu, J.; Bai, H. J.; Zhang, X. B.; Xu, J. J.; Chen, H. Y. *Langmuir*, 2010, 26(2), 1191–1198.
- (5). Hugon, A.; Kolli, N. E.; Louis, C. *Journal of Catalysis*, 274 (2010) 239–250.
- (6). Fritz, N.; Koo, H.; Wilson, Z.; Uzunlar, E.; Wen, Z.; Yeow, X.; Allen, S. A. B.; Kohl, AP. A. *J. Electrochem. Soc.* 159 (6) D386-D392 (2012).
- (7). Jones, M. R.; Osberg, K. D.; Macfarlane, R. J.; Langille, M. R.; Mirkin, C. A. *Chem. Rev.* 2011, 111, 3736–3827.
- (8). Menon, V. P.; Martin, C. R. *Anal. Chem.* 1995, 67, 1920-1928.
- (9). Ahn, W.; Taylor, B; Dall'Asen, A.; Roper, D. K. *Langmuir*, 2008, 24, 4174-4184.
- (10). Ahn, W.; Roper, D. K. *J. Phys. Chem. C* 2008, 112, 12214-12218.
- (11). Blake, P.; Ahn, W.; Roper, D. K. *Langmuir*, 2010, 26(3), 1533.

- (12). Ahn, W.; Roper, D. K. *ACS Nano*, 2010, 4(7), 4181.
- (13). Jang, G. G.; Roper, D. K. *J. Phys. Chem. C*, 2009, 113, 19228.
- (14). Jang, G. G.; Hawkrige, M. E.; Roper, D. K. *J. Mater. Chem.*, 2012,22, 21942-21953.
- (15). Mallory, G. O.; Hajdu, J. B.; *Electroless Plating: Fundamentals and Applications*, American Electroplaters and Surface Finishers Society, Orlando, FL, 1990, ch. 15, pp. 401-420.
- (16). Mallory, G. O.; Hajdu, J. B.; *Electroless Plating: Fundamentals and Applications*, American Electroplaters and Surface Finishers Society, Orlando, FL, 1990, ch. 17, pp. 441-462.
- (17). Henglein, A. *J. Phys. Chem.* 1993,97, 547-5471.

II. TIN SENSITIZATION REVIEW

B. INTRODUCTION

The method of depositing nickel on a steel or nickel surface without using an electric current was discovered by Brenner and Riddell [1]. In 1947, they had a detailed study using this chemical reduction method to deposit nickel and cobalt on different surfaces and named it “electroless plating” [2]. Some methods of electroless plating on non-catalytic substrates’ surfaces were proposed, such as applying alkaline solutions, making contact with a more electronegative metal and depositing a catalytic metal layer on the surface of the non-catalytic metal [2]. Meanwhile, the adhesion property of the deposited metal on different surfaces was also discussed later [2]. The adhesion of the deposits to the steel could be enhanced by an anodic treatment of the steel in concentrated sulfuric acid [2]. The method of using stannous chloride, SnCl_2 , and palladous chloride, PdCl_2 , solutions as an electroless plating catalyst was not developed until 1950 by Bergström [3]. This method was claimed able to metallize all kinds of surfaces that did not reduce stannous chloride, such as glass [3]. There have been a large number of studies of the tin sensitization and palladium activation steps since their discovery. Marton and Schlesinger studied the nucleation and initial growth of the nickel-phosphorous, Ni-P, film by the SnCl_2 - PdCl_2 catalyzing on dielectric substrates [4]. It was found the SnCl_2 - PdCl_2 catalyzing treatment of the substrates created small catalytic sites, and the average diameter of the catalytic sites was estimated at 10 Å [4]. The number of the catalytic sites per unit surface area was found to be related to the hydrophobicity of the substrates: the more hydrophilic the substrates the more the catalytic sites [4]. Based on the SnCl_2 - PdCl_2 activation process, Feldstein et al. compared two different electroless nickel plating baths, and discussed the inhibition effects of various anions in the electroless plating baths, and investigated the metal-to-phosphorus ratio

and different accelerators affecting the electroless plating baths [5-7]. The advantages of the electroless plating method were summarized as a) obtaining uniform deposits over irregular surfaces, b) direct deposition on nonconductors, c) flexibility of deposition on isolated areas, d) desirable characteristics of less porosity and more corrosion-resistance and unique deposit properties, e) applicability for bulk plating [8]. Therefore, the technology of electroless plating is still playing an important role in both industry and academia research.

In this review we discussed the characteristics of the tin sensitized substrates, the conditions for proceeding electroless plating, the mechanism of electroless plating method, and the application of the method. Both the conventional two-step catalyzing system and the single-step catalyzing system were discussed.

C. CHARACTERISTICS OF TIN SENSITIZED SURFACES

Different characteristics of the tin sensitized substrates' surfaces were reviewed in this section. The composition of stannous tin(II) and stannic tin(IV) ions was first discussed. The contact angles, the deposited catalytic sites, and the morphology of the deposited metal were reviewed in the following subsections.

Chemical composition of the tin

Mössbauer spectroscopy study of the colloids centrifuged from the sensitizing solution and the tin on substrates showed identical line positions [9]. Mössbauer spectroscopy is a spectrometry method based on the Mössbauer effect, which was discovered by Rudolf Mössbauer in 1957. The spectrum shows a dip when the resonance absorption appears (the emitting (the gamma source) and the absorbing (the sample) nuclei were in identical chemical environment). The Mössbauer spectroscopy results indicated the tin colloids in the solution were in the same form as the tin on the substrates, and the tin colloids adhered to the substrates when

the substrates were immersed into the solution [9]. Radiochemical tracer adsorption measurements showed the ratio of tin(II) to tin(IV) on Teflon substrate was estimated at 3:1 after sensitization (step one in solution with tin(IV) concentration 25 mM for 1.0 min, step two in solution with tin(II) concentration 0.13 to 0.26 M for 1 to 15 min) [10], which was different from the value found by tin sensitization on Kepton 1:2 (which used solution with only tin(II) concentration at 46 mM) [9]. The difference could be from different substrates, different concentrations, different solutions or different measurement methods.

Contact angle measurement

Concentration, time, and addition of tin(IV) in sensitization solution are important parameters that could affect the contact angle of the tin sensitized substrates. The minimum contact angles for different substrates and different solutions were summarized in Table I. Feldstein and Weiner reported that by measuring the contact angle of the sensitization solutions the effectiveness of the tin sensitization solution could be quantitatively evaluated [11]. By varying the concentrations of tin(II) chloride (from 0 to 0.39 M) and tin(IV) chloride (from 0 to 0.013 M), it was found that at a certain ratio of tin(II) to tin(IV), the contact angle reached 3 different minimum values on 3 different substrates, which represent the best sensitization [11]. The minimum contact angle and the corresponding tin(II) to tin(IV) ratio were found to vary with different substrates and different tin(IV) concentrations. For example, a minimum contact angle of 54° was reported on AZ-1350 resist (positive photo resist from Shipley company) with a sensitization solution of tin(IV) 0.013 M and tin(II) about 0.18 M [11]. H⁺ concentration in tin sensitization solution was found to tend to increase contact angle and excess amount of tin(II) ions relative to tin(IV) ions decreased the rate of tin(IV) ions adhering to the AZ-1350, KTRF and Teflon surfaces [11]. Contact angle measurement of tin sensitization on TiN substrates at

different SnCl₂ and HCl concentrations found increasing the SnCl₂ concentration would increase the contact angle, and the HCl concentration would not affect the contact angle [12]. While increasing the sensitization time, the contact angle decreased at the beginning 3-5 min, then stabilized after 5 min [12]. Another interesting point was that increasing the tin(IV) chloride concentration in the tin(II) and tin(IV) sensitization solution would decrease the minimum contact angle, but not until the contact angle reached 53° for the AZ-1350 resist [11]. Addition of the aged tin(IV) chloride solution into the conventional tin sensitization solution was studied in detail by contact angle, spectral absorption, conductance and nephelometric measurements of the solutions [13]. It was found that the tin(II) and tin(IV) mixture solution had a higher absorption value than the addition of the two separately measured absorption values of the tin(II) and tin(IV) solutions [13]. This non-additive absorption of light by the same element with two different oxidation states was regarded as being due to vibration of electrons between the atoms between the two different oxidation states [13].

Table I. Minimum contact angle for different substrates and different solutions

Ref	Substrates	Contact angle (°)	SnCl ₂ (mM)	HCl (mM)	SnCl ₄ (mM)	Use Aged SnCl ₄ (mM)/(h)	Immersing time (min)
11	AZ-1350 resist	54	260	940	7.5	0	1
11	Teflon	20	130	470	7.5	0	1
11	KTFR resist	17	260	940	13	0	1

13	AZ-1350 resist	37	130	470	7.5	100/60	na
12	TiN	15	55	1233	0	0	na
AZ-1350 positive photo resist from Shipley company. KTRF negative photo resist from Eastman Kodak company. Teflon fluorocarbon film from du Pont. TiN film was made by physical vapor deposition.							

Catalytic sites

The size and density of the catalytic sites after tin sensitization and PdCl₂ activation were found to be related to the addition of aged SnCl₄ solution, and the HCl concentration in the SnCl₂ solution. The higher the HCl concentration used, the smaller the catalytic sites and the higher the density (Table II). The catalytic particle formation was proposed due to the redox reaction between tin(II) and palladium(II). The efficiency of the redox reaction between tin(II) and palladium(II) in which the stannous ion was reduced and the palladium was reduced, during the activation step was proposed to be at most 25% [10]. Electron microscope studies showed that incorporation of an aged (1 week at 25°C) stannic component into the conventional tin sensitization solution formed finer and denser copper crystallites during the initial stage of nucleation [14]. The Pd catalytic particle density increased from 1000 to 10000 particles/μm² [14]. HRTEM study of the conventional two-step activation (SnCl₂ sensitization followed by PdCl₂ activation) on tantalum nitride (TaN) surface found the Pd catalytic sites were 5-10 nm in size [15]. Field emission scanning electron microscope (FESEM) study of the two-step Sn-sensitization and Pd-activation catalyzing system on a TiN surface found the Pd catalytic particle density was at 350 particles/μm² and the catalyzing particle diameter was 48.9±0.3 nm if the Sn-

sensitization step was skipped [12]. When Sn-sensitization with HCl concentration 30 ml/L was applied before the Pd-activation step, the catalyzing particle density was $640/\mu\text{m}^2$ and the particle diameter was 28.2 ± 0.3 nm. While if the HCl concentration increased to 60 ml/L, the catalyzing particle density increased to 1910 particles/ μm^2 and the particle diameter decreased to 16.1 ± 0.1 nm [12].

Table II. Catalytic particle size and density

Ref	Size (nm)	Density (particles/ μm^2)	Substrates	Method
14	2-3	1000	Glass coated with Formvar	SnCl ₂ (0.53mM) HCl (0.1cc/l) sensitization followed by PdCl ₂ (0.56mM) activation
14	2-3	10000	Glass coated with Formvar	Aged SnCl ₄ (5mM) presensitizing followed the same process as the first case (SnCl ₂ +PdCl ₂)
15	5-10	na	TiN	SnCl ₂ (53mM) with HCl (40ml/L) then activation PdCl ₂ (1.4mM) with HCl 2.5ml/L)
12	48.9	350	TiN	Only PdCl ₂ (0.56mM) with HCl (3.0ml/L) and HF (5.0ml/L)
12	28.2	640	TiN	SnCl ₂ (36.8mM) HCl (30ml/L) followed by the formal only PdCl ₂ process
12	16.1	1910	TiN	SnCl ₂ (36.8mM) HCl (60ml/L) followed by the formal only PdCl ₂ process
Formvar is coated by solution with 4g polyvinylformal in 1liter ethylene dichloride.				

Metal deposition island morphology

Tin sensitization solution was found to have big effects on the nucleate site size and film roughness in the final electroless plating step. Schlesinger and Kisel studied 11 sensitizers for electroless plating on glass surface (Table III) [16]. Using aged sensitizer solution (stannous chloride) decreased the nucleate size from 140 nm to 4.5 nm. With the addition of different surfactants the nucleate sites decreased in size: for example, Triton X-100 reduced the size to 95.3 nm. They found a relationship of a higher than linear increase between the sensitizer adsorption (mg/m^2) and the number of metal islands ($\text{particles}/50 \text{ nm}^2$); and for a given sensitizer the higher the density of the nucleation site, the smaller the size of the nucleated island when its property was changing with time [16]. Atomic force microscopy (AFM) study of Ag electroless plating film found tin sensitization affected the roughness of the deposited films [12]. The root mean square (RMS) roughness was 7.71 nm for TiN surface treated with only PdCl_2 activation step, then decreased to 7.31 nm for TiN surface with SnCl_2 (with 30ml/L HCl) sensitization and PdCl_2 activation, and became 4.66 nm when the HCl concentration in SnCl_2 increased to 60 ml/L [12].

Table III. Nucleate size with different sensitization solutions Ni plated for 1 min [16]

	Sensitizer	Aging (h)	Nucleate size (nm)
1	0.1M SnCl_2 and 0.1M HCl	0	140.6
2	#1	48	29.7
3	#1	96	11.2
4	#1	144	4.5
5	#1	288	8.1

6	#1 plus 10mg/L hydroquinone	3	80.6
7	#1 plus 10mg/L hydroquinone	48	39.7
8	#1 plus 10mg/L thiourea	24	7.6
9	#1 plus 10mg/L thiourea	72	17.2
10	#1 plus 0.05 _{wt} % triton X-100	0	95.3
11	#1 plus 0.05 _{wt} % triton X-100	240	4.9

D. CONDITIONS TO PROCEED TIN SENSITIZATION

The chemistry of the tin sensitization solution and its improvement became interesting topic to scientists, after the tin(II) sensitization solution was used in electroless plating process. Tin(II) deposition on substrates was proposed to come from air oxidation and hydrolysis of tin(II) chloride and precipitation of soluble tin in a colloidal form during washing due to pH increase [17]. Based on this mechanism, it was proposed that tin sensitization could be affected by the solution pH, concentration and aging [17]. Meanwhile, it was demonstrated that the tin sensitization system was independent on immersion time (after 5 min), concentration of aged tin(IV) (between 5 and 50 mM), and concentration of tin(II) (between 0.13 and 0.26 M) [10].

Aging solution

Applying aged SnCl₄ in the SnCl₂ sensitization solution was found able to enhance electroless plating by contact angle measurement, catalytic site study, and mechanism discussion. The sensitization solution with aged tin(IV) chloride solution in the tin sensitization solution was found able to improve the sensitization process in 1972 [13]. Table I showed the addition of aged SnCl₄ led to the contact angle drop from 54° to 37°. Meanwhile, Table II demonstrated that when applying aged SnCl₄ the density of catalytic sites was 10 times the others.

The transformation of α -stannic acid (hydrolyzed tin(IV) chloride form) to β -stannic acid (a polymeric form with proposed formula of $(\text{HO})_3\text{-Sn-[O-Sn-(OH)}_2\text{]}_n\text{-OH}$ or $(\text{HO})_2\text{-Sn-[O}_2\text{Sn]}_n\text{-(OH)}_2$) was proposed during the aging process [13]. Increasing the β -stannic acid concentration improved the tin sensitization solution performance [13]. It was also found that increasing temperature and decreasing stannic concentration in the aging process would accelerate β -stannic acid formation. Diluting the solution increased the stannic hydrolysis and higher temperatures increased the reaction rate (hydrolysis and polymerization) [13]. While high acid (HCl) content and high sodium chloride concentration would inhibit the α - to β -stannic acid transformation [13]. It was found that applying an aged stannic component improved the affinity for catalyst adsorption onto organic surfaces, and the stannous ions interacted with the stannic component reacted with PdCl_2 to form catalytic sites for electroless plating [13, 18]. Tin(II) oxidation, complex formation, tin(II) and tin(IV) hydrolysis, and aging of the sensitization solution were discussed by Przyłuski et al [19]. Study of the tin sensitization solution aging found that in the initial stage (0-50 hr) the oxidation and complex formation processes were predominant, after 500 hr the hydrolysis process became predominant [19]. It was observed that the tin(II) and tin(IV) complex had a maximum absorption between wavelength 345 and 360 nm and the formula for the complex was proposed as $[\text{Sn}^{\text{II}}_3\text{Sn}^{\text{IV}}\text{Cl}^{\text{I}}_n]^{14-n}$ [19]. It was also found the tin(II) oxidation in air followed a zero-order reaction mechanism and the oxidation rate was determined by the oxygen molecules penetrating through the air-solution interface [19].

Substrates

Contact angle measurement, Mössbauer spectroscopy, radiotracer analysis, X-ray photoelectron spectroscopy (XPS), and other analytical methods were used to examine properties of different substrates after sensitization and activation. The contact angles were measured on

AZ-1350 resist (positive photoresist, Shipley Company), KTFR resist (negative photoresist, Eastman Kodak Company) and Teflon (fluorocarbon film, trade mark of E. I. du Pont de Nemours & Co.) substrates after tin sensitization in different tin(II) to tin(IV) ratio and shown in Table I [11]. The results showed Teflon substrate was the most sensitive substrate to the tin(II) to tin(IV) ratio and both Teflon and KTFR resist had a minimum contact angle at around 17° that was much lower than AZ-1350 resist (about 53°) [11]. A Mössbauer spectroscopy study of tin sensitization on Kapton (du Pont polyimide) showed the tin(II) to tin(IV) ratio on the substrate was 1:2 and the tin to palladium ratio was 3.8:1 after the Pd catalyzing step [9]. Tin sensitization on graphite surfaces was studied by Meek and Cohen with Rutherford scattering technique and Mössbauer spectroscopy [20]. The Pd-Sn alloy formation at the catalytic centers in single-step sensitization system was confirmed [20]. Rutherford backscattering analysis found Sn:Pd ratio was 2:1 on Si_3N_4 substrates by single-step Pd-Sn sensitization [21]. Using radiochemical tracer analysis and proton backscattering analysis, a Pd concentration of 3.4×10^{14} atoms/cm² and 3.25×10^{14} atoms/cm² were reported respectively after the sensitization and activation steps on soda lime glass substrates [22, 23]. On the other hand, XPS study on tin sensitized and silver activated soda lime glass showed the Sn:Ag ratio was about 1:2 [24]. Tin concentration of 0.71×10^{15} atoms/cm² was found by X-ray fluorescence spectroscopy (XRF) after tin sensitization on alumina substrates [25].

Electroless Cu plating was studied on epoxy substrates [26]. It was found that applying NaOH and EDTA accelerators generated the most uniform Cu films [26]. The reason was proposed as after the accelerators' step, the stannous out layer was removed and the catalytic sites were exposed to the solution (read the mechanism section for detail). HRTEM study of the conventional two-step activation (SnCl_2 sensitization followed by PdCl_2 activation) on tantalum

nitride (TaN) surface found the Pd catalytic sites were 5-10 nm in size [15]. Field emission scanning electron microscope (FESEM) study of the two-step Sn-sensitization and Pd-activation catalyzing system on TiN surface found the Pd catalytic particle density was at 350 particles/ μm^2 [12].

E. TRIFLUOROACETIC ACID (TFA) IN TIN SENSITIZATION SOLUTION

Trifluoroacetic acid (TFA) was found to be able to replace the conventional HCl for tin sensitization solution. The application of trifluoroacetic acid (TFA) in the tin sensitization solution was first appeared in Martin's report [27]. Although in 1994 the conventional tin-HCl solution was used in Martin's report as a sensitization solution for electroless silver and gold plating, Menon and Martin applied a solution with 0.07M TFA and 0.026 M SnCl_2 for the sensitization step for electroless metallization of membrane in a report in 1995 [27, 28]. The tin-TFA sensitization solution pretreatment was applied to silica spheres and achieved homogeneous deposition of silver nanoparticles [29]. Applying the tin-TFA sensitization and controlling Au deposition time allowed production of ultrathin uniform Au (111) films with enhanced features relative to sputtered Au films [30]. Base on the tin-TFA sensitization and silver activation steps, regular arrays of Au NPs can be made by depositing metal onto a pattern created by top-down electron (e)-beam lithography [31] or by bottom-up nanosphere self-assembly [32]. Using continuous flow to maintain a constant thermodynamic driving force and enhance mass transfer rates to the surface improved the Au film quality and enhanced its optical features with the same tin-TFA sensitization, Ag activation and Au plating solutions [33]. Real-time transmission UV-vis (T-UV) spectroscopy was recently used to characterize disposition and dynamics of Ag disposition during and after Ag reduction onto the tin(II) sensitized surface during continuous flow [34]. Ag nanoparticle formation as catalytic sites for electroless gold plating was

dynamically recorded by T-UV spectra [34]. Tin-TFA sensitization may have some limitations, such as less tin(II) on the substrates, the production of large grain size, and higher pK_a than HCl (pK_a of TFA is 0.23, pK_a of HCl was -7.0).

F. PHOTO SELECTIVE METAL DEPOSITION (PSMD)

The PSMD method based on the tin(II) and tin(IV) sensitization process was popularly applied for selective metal deposition used in photolithography. It was reported that the selection of positive or negative PSMD could be controlled by simply adjusting the bath pHs for electroless Ni plating [35]. The micro-scale metal patterns were fabricated on polyimide film by selectively oxidizing the tin(II) on the substrates with UV light irradiation [36].

Idea development

The idea of photo selective metal deposition (PSMD) by combining the conventional electroless plating method (SnCl_2 - PdCl_2 activated) with an ultraviolet radiation treatment under a photo mask was first carried out by Sharp [17]. The procedure was proposed as follows (Figure I). First, the substrate was covered with a layer of divalent tin after sensitized in SnCl_2 . Second, the divalent tin would be oxidized to tetravalent tin when exposed to ultraviolet radiation; while the surface, covered by a photo mask, would remain in the divalent tin form. Third, the Pd(II) in activation solution would be selectively reduced on the divalent tin surface and form the Pd catalytic sites. Finally, the metal was selectively deposited by electroless plating on the substrates where the Pd catalyst was deposited [17]. The mechanism of the divalent tin(II) oxidized by ultraviolet radiation was first studied by Cohen et al. using the Mössbauer spectroscopy [9]. They found that the divalent tin on the surface would be oxidized to the tetravalent form, when the SnCl_2 sensitized substrates were either exposed to UV light or immersed in a PdCl_2 -HCl solution [9].

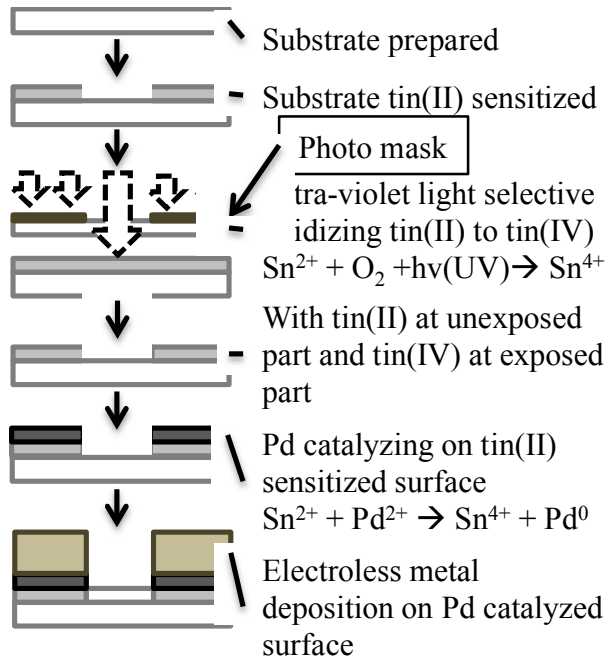


Figure I. Photo-selective Metal Deposition process [17].

Mechanism discuss

The mechanism was improved by Chow et al., who studied the application of UV light after sensitization and after activation for electroless plating of Cu, Ni and Co [37]. It was found that for all three of the metals (Cu, Ni and Co), plating would be inhibited as expected because of the tin(II) to tin(IV) oxidation reaction if the UV light was applied after the tin sensitization step; however, when the UV light was applied after the activation step, the electroless Ni and Co plating were still inhibited [37]. The reason was proposed as follows [37]. Phosphorus was involved in the Ni and Co deposition solution, which would increase the degree of crystallization of the Pd catalyst in UV irradiation and inhibit the electroless Ni and Co plating. On the other hand, hydrogen was incorporated in electroless Cu film deposition, which would not inhibit the deposition. Later, it was found that Cu deposition could possibly be inhibited by UV light irradiation after activation, if the water rinse times between sensitization, activation, and metallization were shorted to 15 sec [38]. The idea of using UV light to inhibit electroless plating

was also tested on plastic substrates, and the most effective inhibition was obtained from applying UV light just after the catalyzing step [39].

Using tin(IV) chloride solution as a sensitizer, Baylis et al. provided a novel way of UV light inhibiting electroless plating [40]. They found using tin(IV) sensitization and Pd activation, the electroless Ni plating would still work and the plating would be inhibited if UV light was applied after the Pd activation [40]. However, electroless Cu plating was different: the Cu was only deposited when the UV light was applied after the Pd activating step [40]. It was proposed that the Pd catalyst was generated from the light induced reduction of Pd(II) to Pd(0) on the Sn(IV) sensitized substrate [40]:



It was proposed again that UV light irradiation could increase the degree of crystallization of Pd catalyst in the presence of phosphorus and inhibit electroless Ni plating. This hypothesis reinforced the UV light inhibition mechanism first proposed by Chow et al. mentioned earlier [37]. Electroless Co and Ni plating in alkaline baths were also studied by Baylis et al. for photo-selective metal deposition (PSMD) with a tin(IV) sensitizer [41]. It was found that the reduction of Sn⁴⁺-Pd²⁺ to Sn⁴⁺-Pd⁰ catalyst could only happen in acidic conditions, because Pd²⁺ was converted to Pd(OH)₂ in a basic solution which had a lower reduction potential than the PdCl₂ form in the acid solution [41].

However, the mechanism of UV light irradiation inhibition in electroless plating was still in debate. Five different ways that UV light could possibly affect the Pd catalyst were proposed; they were: (a) UV light reduced Pd²⁺ to Pd⁰; (b) UV light with air oxidizing Pd²⁺ to Pd⁴⁺; (c) UV

light rendered Pd⁰ site non-catalytic; (d) UV light breaking the bonds connecting the Pd catalyst to the substrate; (e) UV light dehydrating the Pd²⁺ and forming insoluble palladium oxide [42]. In order to clarify the mechanism, the Pd²⁺ on substrates and in rinse water from different ways of tin sensitization and UV light irradiation was quantified by a spectrophotometric method [42]. More Pd²⁺ was recovered in the rinse water after UV irradiation on the dried substrates, compared to the non-UV irradiation one. Based on the experimental results, the hypothesis was proposed that the theory that UV light reduced Pd²⁺ to Pd⁰ was not true if Pd⁰ was the catalyst, because in this way the concentration of Pd²⁺ in rinse water after UV irradiation should be lower; and that the theory that UV light broke the bond between the Pd catalyst and the substrate was not appreciated, because in that case the Pd catalyst in the rinse water would still be effective for electroless plating; however, in experimentation it was not [42]. Even though the mechanism of tin(IV) sensitization for PSMD was still not completely uncovered [35], the method for selective Ni and Co electroless plating [41] were duplicated by different groups.

G. SINGLE-STEP TINSENSITIZATION

The single-step tin sensitization process was developed for its convenience and greater efficiency. It would provide more reproducible results if the catalyzing solution was stabilized. The catalyst particle size was smaller (3 nm) than the conventional two-step process (Table II). However, the disadvantage was that accelerators (HCl, NaOH or others) had to be applied to improve the efficiency of the catalysts.

Method development and comparison with two-step system

Other than the conventional two-step surface activation method (tin sensitization followed by palladium activation), a single-step catalyzing method with Sn-Pd complex was developed and studied. Scanning tunneling microscopy (STM) was used to characterize the Pd

catalytic clusters on graphite substrates [43]. A pyramidal cluster with 40 Pd atoms (4×5 atom basis) was proposed [43]. A Mössbauer spectroscopy study of the single-stage Sn-Pd complex treatment solution proposed that the stoichiometry of the complex could be $\text{Pd}^{2+}\text{-3Sn}^{2+}$, that the complex was unstable and auto-reduced to a Sn-Pd alloy, and that excess tin(II) ion in solution formed a monolayer of stannous shell on the particle which stabilized and limited the catalyst particle size [44]. Meek found that the two-step sensitization process (tin(II) sensitization and followed by palladium(II) activation) was basically different from the single-step Sn-Pd complex solution system by a Rutherford scattering study [45]. The former two-step sensitization process showed a lower Pd/Sn ratio, more Pd and Sn species lost into the electroless plating solution, and a longer time required to initiate the electroless plating reaction [45].

Combined Mössbauer spectroscopy with electron microscopy and a Rutherford backscattering study of the Sn-Pd complex solution sensitizing graphite substrates by Cohen and Meek showed the catalytic sites for electroless plating were suspensions of colloidal particles of Sn-Pd alloy with an upper limit particle size of about 30 Å in diameter (see Figure II) [20]. Single-step sensitization solution with tin(IV) was also developed for photo selective metal deposition (PSMD) and the effective lifetime of the sensitization solution was improved from 45 hours to 3 months by adding HCl to slow down tin(IV) chloride hydrolysis [40, 46]. High-resolution transmission electron microscopy (HRTEM) study of the single-step Pd-Sn catalyzing showed the solution temperature, colloid growth time, and solution aging time were critical factors that determined the catalytic particle sizes [21]. The catalytic core prepared in concentrated acidic media at room temperature was found to have a low tin concentration, and aging the catalyst improved the nucleus crystalline organization [21]. Heating or increasing the

pH of the catalytic solution during the colloid formation was found to produce highly crystallized tin-rich catalytic sites [21].

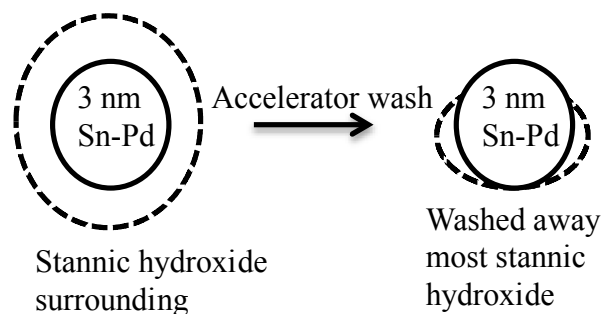


Figure II. Proposed structure of the Pd-Sn alloy catalytic site [20].

Accelerator

Applying accelerator after single-stage sensitization would improve the catalytic efficiency [44]. An electron microscope study of the single-step sensitization showed either application of the accelerator solution or addition of the aged tin(IV) solution to the catalyzing solution would improve the surface catalyzing process [47]. Energy dispersive spectroscopy (EDS) analysis of different accelerator steps affecting single-step Pd-Sn catalyzed graphite-epoxy composite substrates found acceleration with NaOH (0.5 M) removed an equivalent amount of Sn as the electrochemical method (potential greater than 1.0 V vs. reversible hydrogen electrode (RHE)), which was much better than HCl (8%) accelerator [48]. In another study, five different accelerators (NaOH, HCl, H₂SO₄, NH₄OH and NH₄BF₄) were compared by TEM and electron diffraction analysis [49]. It was found that the NaOH accelerator produced the finest remaining particles, while the accelerators with ammoniate group (NH₄OH and NH₄BF₄) coagulated small particles to produce high-density particles [49].

Electrochemical method study

Cyclic voltammetric technique study of the tin sensitization solutions showed the concentration of tin(II), tin(IV), and palladium(II) in solutions could be measured within $\pm 10\%$

of accuracy [50]. It was found the tin(II) ion in solution would inhibit the dissolution of the 0 valence palladium(0) and the tin(II) ion on the electrode surface could be leached by rinsing with high chloride concentration solution [50]. The Pd-Sn catalyzing solution (palladium concentration varied from 0.1 to 0.4 mM and tin concentration ranged from 1 to 4 mM) was studied by cyclic and linear voltammetry method [51]. It was found that electrochemical reduction of palladium(II) was a process with two one-electron transfer steps (the diffusion coefficient of palladium(II) was determined as $1.17 \times 10^{-9} \text{ m}^2/\text{s}$), electrochemical reduction of tin(II) in 0.1 M HCl was diffusion limited (the diffusion coefficient was measured by rotation disk electrode as $2.5 \times 10^{-10} \text{ m}^2/\text{s}$), and electrochemical reduction of tin(IV) only happened in solutions with high-HCl concentrations (the hydrolysis dominated at 0.1 M HCl solution, and in 1 M HCl solution the hydrolysis was inhibited) [51].

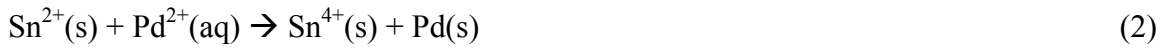
H. TIN SENSITIZATION MECHANISM DEVELOPMENT

The mechanism of tin sensitization and palladium with/or silver activation has been discussed in literature for many years. A widely accepted mechanism was proposed in Figure III. Meanwhile, the mechanism of the single step Sn-Pd activation process was different from the two-step process, and was also discussed.

Conventional two-step system

The mechanism of tin(II) sensitization was considered, and two processes were suggested that could contribute to tin(II) deposition on the substrates: colloid formation in solution due to tin(II) chloride oxidation in air and hydrolysis in water; and precipitation of soluble tin species from the solution during the water rinse step due to rapid pH increase [17]. Therefore, the effectiveness of the tin sensitization step was proposed to be affected by the solution factors such as pH, concentration and aging, substrates' property and pretreatment, and immersing and

rinsing process [17]. A Mössbauer spectroscopy study of tin(II) sensitization on Kapton (du Pont polyimide) showed the ratio of tin(II) to tin(IV) ions on the substrate was about 1:2 and the total amount of tin on the substrate remained at about $10 \mu\text{g}/\text{cm}^2$ before and after the activation step with Pd(II) [9]. After activation, the atomic ratio of tin to palladium was approximately at 3.8:1, which showed the amount of tin(II) oxidized and the amount of the Pd(II) reduced were the same [9]:



A radiochemical tracer analysis study reported that the surface concentrations of tin(II) and tin(IV) on a tin sensitized Teflon substrate were at 1.2×10^{16} atoms/cm² and 0.36×10^{16} atoms/cm² respectively [10]. The tin(II) concentration on tin sensitized soda-lime glass was found between 0.702×10^{15} atoms/cm² in our lab (unpublished result, tin concentration was 26 mM, trifluoroacetic acid concentration was 66 mM, sensitization time was 3 min). A Rutherford scattering study of tin sensitization on cleaved graphite substrates showed that the tin concentration on the surface was at about 1.5×10^{16} atoms/cm², the ratio of O/Sn (the Sn counted for the total amount of tin on the substrate) was about 1.3, and the Cl/Sn ratio was close to 0.1 [45]. After Pd catalyzing the O/Sn ratio increased to 2 and the Pd/Sn ratio was approximately at 0.2, while the Pd/Sn ratio after activation on Kapton found by Mössbauer spectroscopy was about 1:3.8 [9, 45]. Rutherford backscattering analysis of Pd-Sn catalyzing the Si₃N₄ substrate found that the palladium and tin concentration concentrations were at 1.6×10^{15} atoms/cm² and 3.5×10^{15} atoms/cm², respectively [21]. The Pd/Sn ratio was found to increase with the immersion time from 0.3 to 0.5 during the first 5 min, and after 5 min it was stabilized [21]. Introducing an

immersion of the substrates in a silver nitrate solution between the stannous chloride and the palladium chloride steps showed a very homogeneous nucleation [22]:



Radioactive tracer analysis of Sn, Ag and Pd on soda lime glass substrates showed: the total amount of tin after SnCl_2 sensitization and rinsing was about $0.12 \mu\text{g}/\text{cm}^2$ (6.1×10^{14} atoms/ cm^2), the silver concentration followed by AgNO_3 activation and rinsing was about $0.16 \mu\text{g}/\text{cm}^2$ (8.9×10^{14} atoms/ cm^2), and the palladium concentration followed by PdCl_2 and rinsing was about $0.06 \mu\text{g}/\text{cm}^2$ (3.4×10^{14} atoms/ cm^2) [22]. If the AgNO_3 solution was skipped, the Pd concentration was decreased to about $0.04 \mu\text{g}/\text{cm}^2$ (2.3×10^{14} atoms/ cm^2) [22]. Similar Pd concentration (3.25×10^{14} atoms/ cm^2) was reported by applying a proton backscattering analysis of the Pd catalyzed soda lime glass [23]. Baylis et al. suggested a minimum Pd catalyst coverage of 5×10^{13} atoms/ cm^2 in order to initiate electroless metal deposition on glass [23]. An x-ray fluorescence spectrometry (XRF) study quantitatively measured the amount of tin, silver and palladium on the alumina substrates surface after each step [25]. It reported tin 0.71×10^{15} atoms/ cm^2 after tin sensitization, silver 1.3×10^{15} atoms/ cm^2 after silver nitrate intermediate step, and palladium 0.5×10^{15} atoms/ cm^2 after PdCl_2 activation [25]. Because different analysis methods performed in the different regions of the catalytic site, from the core to the shell, the Pd/Sn ratios varied [8]. Table IV summarized all the different tin, silver and palladium concentration previously reported and cited in this review (please read the original paper for detail information).

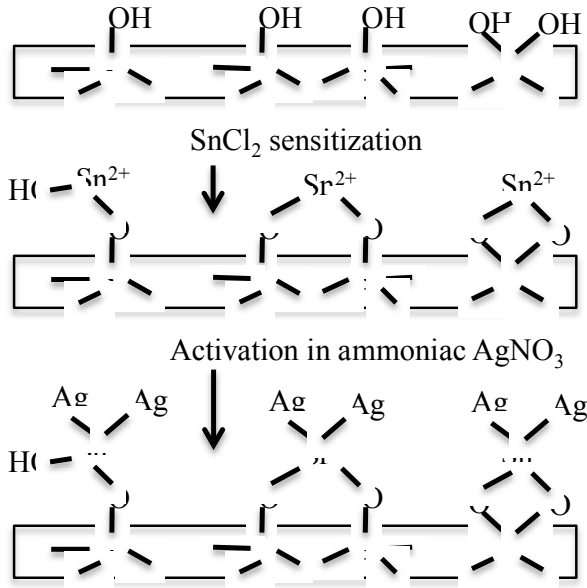


Figure III. Tin sensitization and silver activation on soda lime glass [24].

Table IV. Surface concentration of tin, silver and palladium (atoms/cm²)

Ref	Tin(II)	Tin(IV)	Tin (total)	Ag	Pd	Methods
10	1.2×10^{16}	0.36×10^{16}	na	na	na	Radiochemical tracer
21	na	na	3.5×10^{15}	na	1.6×10^{15}	Rutherford backscattering
22	na	na	6.1×10^{14}	8.9×10^{14}	3.4×10^{14}	Radiochemical tracer
23	na	na	na	na	3.25×10^{14}	Proton backscattering
25	na	na	0.71×10^{15}	1.3×10^{15}	0.5×10^{15}	X-ray fluorescent spectrometry

45	na	na	1.5×10^{15}	na	na	Rutherford backscattering
Our lab	0.702×10^{15}	na	na	na	na	Spectrophotometry

Single-step catalyzing system

The mechanism of a single-step catalyzing system was found with a Mössbauer spectroscopy study of a single-step Sn-Pd complex sensitization on Kapton substrates; it showed a mixture of tin(II) and tin(IV) lines which indicated tin(II) stabilizing the Sn-Pd catalyst [44]. After the ‘accelerator’ washing, the tin(II) line was absent and the catalytic activity of the surface was increased [44]. Based on electron microscopy and electron diffraction study of single-step catalyzing followed by acceleration, Feldstein et al. proposed that the presence of Pd₃Sn prior to the metallization step would produce the best plating results [47]. Another Mössbauer spectroscopy study of tin sensitizing on graphite substrates with a single Pd-Sn complex sensitization solution also found catalytic Pd-Sn alloy formation [20]. The single-step tin sensitization processes were suggested as: first colloidal particles with Pd-Sn alloy adsorption on substrates, second excess stannic hydroxide removal by accelerator (20 ml Shipley 19 in 100 ml water), third additional removal of stannic hydroxide during electroless Cu plating (in the Mac-Dermid 9070D electroless Cu plating solution) [20].

A TEM study of Pd-Sn catalyst system showed the high catalytic activity was due to large colloidal particles, and the accelerator (1 M NH₄BF₄ or 1:1 HCl) caused coagulation of small particles that increased activity [52]. X-ray photoelectron spectroscopy (XPS) showed the Pd/Sn ratio was not constant for particles with different catalytic activities, and the Pd and Sn could exist as Pd-Sn intermediate or alloys [52]. Another study found the Pd/Sn ratio was ~0.3

before acceleration, increased to ~ 1 after HCl acceleration and >2 when NaOH was accelerated [26]. Another XPS study of SnCl₂ and SnCl₄ sensitization (both concentrations were 2.5 mM) on soda lime glass surfaces found that the tin coverage were the same between 1: 5 and 1:10 (Sn:Si) [24]. After the tin(II) and tin(IV) sensitized glasses were treated in ammoniac silver nitrate solution, the Ag to Sn ratio on the glass surface were estimated at 2.3 [24]. It was higher than the former ratio 1.6 measured by radioactive tracer analysis, because in the former case the SnCl₂ concentration was lower (0.44 mM) [22, 24]. The mechanism of tin sensitization and silver activation were concluded in Figure III [24]. A more detailed discussion of single-step activation process is in the single-step tin sensitization section.

I. APPLICATION OF TIN SENSITIZATION

Tin sensitization is used for deposition metal on different substrates. Depending on the metal and the substrates, it could be used in microcircuits, electronics, solar cells, and catalysts. Following the steps of SnCl₂ solution sensitization, rinse, PdCl₂ activation, and rinse, the electroless plating of Ni, Ni-Co alloy, and Co was studied [4, 53]. It was proposed the structure of Co deposited could be either (face centered cubic) fcc or (hexagonal close packing) hcp, while the Ni and Ni-Co alloy films were in fcc structures [53]. Addition of aged SnCl₄ to the conventional SnCl₂/HCl sensitization solution improved the sensitizer by showing higher island density and uniformity of the deposit for electroless plating of Ni [54]. The resistivity of the 80 nm thick Ni with boron (20-30_{atom}%) film (Ni-B) dropped from 10⁵ μΩ/cm to 10² μΩ/cm when the deposited film was heat treated at 40°C [54]. Pd-Sn catalyst fabricated by cyclic voltammetry and conoamperometric binary electro-deposition was studied for nitrate reduction [55]. It was reported the best catalytic performance was at the ratio of Pd₃₀Sn₇₀ [55]. An XPS study of the electrodeposited film found the average surface composition was 50-60% Sn, 40-50% SnO, and

60-70% Pd, 30-40% PdO for all the films with different Pd/Sn ratios [55]. Recently Zabetakis and Dressick discussed selective electroless metallization of patterned polymer films for fabrication of electrical interconnects, plasma-etch-resistant masks, and diffusion barriers in electronics [56]. They described the fabrication of ~50 nm width features in metal for current industry design and the challenges of fabrication of sub 10 nm metal features [56]. Using stannous chloride as both a reducing and stabilizing agent, John et al. reported a new method to synthesize Pt catalytic clusters with less than 20 atoms [57]. An Sn/Ag catalyst was investigated as a cost-efficient replacement of Sn/Pd catalyst for electroless plating of silver and copper on epoxy-based polyhedral oligomeric silsesquioxane (POSS) films [58]. Using SnCl₂-HCl solution for sensitization and Pt colloid solution as activation, tunable shell thickness (35-198 nm) of Ag film was coated on polystyrene (PS) microspheres [59]. Au deposited glass sensor for solution dielectric constant measurement was fabricated by tin-TFA solution sensitization, silver ammoniac nitrate solution activation and Oromerse Part B solution Au plating on sodium glass plate [60].

J. CONCLUSION

Different characteristics of the tin sensitization process were summarized. The chemical composition of the tin sensitized substrates was found to have different ratios of tin(II)/tin(IV) (varied from 3:1 to 1:2). The difference could come from the solution concentration or different analytical methods. Contact angle measurement of different tin sensitized surfaces showed that different substrates, concentrations and solution aging determined contact angles. AZ-1350, Teflon, KTFR substrates showed different contact angles: 54°, 20°, 17° respectively; and the addition of aged SnCl₄ decreased the contact angle on AZ-1350 substrate to 37°. The catalytic sites' diameter and density were found related to the HCl concentration in the sensitization

solution and the addition of aged SnCl₄ solution. By increasing the HCl concentration from 0 to 60 ml/L, the catalytic particle size decreased from 48.9 nm to 16.1 nm, and the density increased from 350 particles/μm² to 1910 particles/μm². The addition of aged SnCl₄ increased the density of the catalytic sites by 10 orders of magnitude. The surfactants were also found to have an important effect on the sensitization solution by studying the morphology of the deposited metal. The 144 h aged sensitizer showed the minimum nucleate size at 4.5 nm; the addition of Triton X-100 decreased the nucleate size from 140.6 nm to 95.3 nm without aging; the addition of hydroquinone at 3 h aging had an 80.6 nm nucleate size; and by adding thiourea and aging the solution 24 h, the catalytic size was at 7.6 nm.

Conditions that could affect the tin sensitization process were aging SnCl₄, different substrates, acid usage (switching HCl to trifluoroacetic acid), UV light exposure and single-step sensitization. Applying aged SnCl₄ was found to enhance the absorption of tin(II) and therefore improve electroless plating. TFA was found to be a good surfactant and producing an acidic environment to avoid tin(II) hydrolysis. A photo selective metal deposition (PSMD) method was developed based on UV light-induced catalyst inhibition. Different metal patterns were fabricated by the PSMD method; however, the mechanism was found to be different for different electroless plating systems, and is still in debate. The single-step tin sensitization with an activation step was found to be another effective process for producing catalyzed surfaces.

The mechanism of the sensitization and activation steps was studied in detail by different methods. Based on the concentration of the tin and Pd (or with Ag) on the substrate during each step, a widely accepted mechanism was proposed. The divalent tin compound was first absorbed on the substrates by tin sensitization, the palladium(II) or silver(I) would be reduced following a redox reaction mechanism and become a catalytic site, and the electroless plating could then

happen on the catalytic sites. Figure III illustrates the process of Ag catalyst deposition on glass substrate. The current application of the tin sensitization method could be in fabricating metal film for microcircuits, solar cells, and in making catalysts.

K. REFERENCES

- (1). A. Brenner and G. E. Riddell, *Research Paper RP1725.*, **37** (1946).
- (2). A. Brenner and G. E. Riddell, *Research Paper RP1835.*, **39** (1947).
- (3). E. A. Bergström, *US Patent.*, **193532**, 2702253 (1955).
- (4). J. P. Marton and M. Schlesinger, *J. Electrochem. Soc.*, **115**, 1 (1968).
- (5). N. Feldstein, *RCA Review.*, **31** (1970).
- (6). N. Feldstein and P. R. Amodio, *J. Electrochem. Soc.*, **117**, 9 (1970).
- (7). N. Feldstein and T. S. Lancsek, *J. Electrochem. Soc.*, **118**, 6 (1971).
- (8). B. Viswanathan, *Current Science.*, **65**, 7 (1993).
- (9). R. L. Cohen, J. F. D'Amico and K. W. West, *J. Electrochem. Soc.*, **118**, 12 (1971).
- (10). N. Feldstein and J. A. Weiner, *J. Electrochem. Soc.*, **120**, 4 (1973).
- (11). N. Feldstein and J. A. Weiner, *J. Electrochem. Soc.*, **119**, 6 (1972).
- (12). H. Koo, S. Y. Kim, S. K. Cho and J. J. Kim, *J. Electrochem. Soc.*, **155**, 9 (2008).
- (13). N. Feldstein, J. A. Weiner and G. L. Schnable, *J. Electrochem. Soc.*, **119**, 11 (1972).
- (14). N. Feldstein, S. L. Chow and M. Schlesinger, *J. Electrochem. Soc.*, **120**, 7 (1973).
- (15). Y. Sung, C. Lai, S. Lin and Chang Shou-Yi, *Electrochemical and Solid-State Letters.*, **9**, 5 (2006).
- (16). M. Schlesinger and J. Kisel, *J. Electrochem. Soc.*, **136**, 6 (1989).
- (17). J. F. D'Amico, M. A. De Angelo, J. F. Henrickson, J. T. Kenney and D. J. Sharp, *J. Electrochem. Soc.*, **118**, 10 (1971).
- (18). N. Feldstein, *Plating in the electronics industry.*, (1973).

- (19). J. Przyłuski, M. Kasprzak and J. Bieliński, *Surface and Coatings Technology.*, **31**, 3 (1987).
- (20). R. L. Cohen and R. L. Meek, *Journal of Colloid and Interface Science.*, **55**, 1 (1976).
- (21). M. Froment, E. Queau, J. R. Martin and G. Stremmsdoerfer, *J. Electrochem. Soc.*, **142**, 10 (1995).
- (22). C. H. de Minjer and v.d. Boom, P. F. J., *J. Electrochem. Soc.*, **120**, 12 (1973).
- (23). B. K. W. Baylis, N. E. Hedgecock, M. Schlesinger and A. van Wijngaarden, *J. Electrochem. Soc.*, **126**, 10 (1979).
- (24). L. R. Pederson, *Solar Energy Materials.*, **6**, 2 (1982).
- (25). J. W. Severin, R. Hokke, H. van der Wel and G. de With, *J. Electrochem. Soc.*, **140**, 3 (1993).
- (26). J. Horkans, J. Kim, C. McGrath and L. T. Romankiw, *J. Electrochem. Soc.*, **134**, 2 (1987).
- (27). V. P. Menon and C. R. Martin, *Anal. Chem.*, **67**, 13 (1995).
- (28). C. J. Brumlik, V. P. Menon and C. R. Martin, *J. Mater. Res.*, **9** (1994).
- (29). Y. Kobayashi, V. Salgueiriño-Maceira and L. M. Liz-Marzán, *Chem. Mater.*, **13**, 5 (2001).
- (30). W. Ahn, B. Taylor, A. G. Dall'Asen and D. K. Roper, *Langmuir.*, **24**, 8 (2008).
- (31). P. Blake, W. Ahn and D. K. Roper, *Langmuir.*, **26**, 3 (2010).
- (32). W. Ahn and D. K. Roper, *ACS Nano.*, **4**, 7 (2010).
- (33). G. Jang and D. K. Roper, *J. Phys. Chem. C.*, **113**, 44 (2009).
- (34). G. Jang, M. E. Hawkrigde and D. K. Roper, *J. Mater. Chem.*, **22** (2012).
- (35). I. Kiflawi and M. Schlesinger, *J. Electrochem. Soc.*, **130**, 4 (1983).
- (36). J. Y. Kim, T. V. Byk, S. H. Cho, C. Noh, K. Y. Song, J. M. Kim and T. V. Gaevskaia, *J. Electrochem. Soc.*, **9**, 12 (2006).
- (37). S. L. Chow, N. E. Hedgecock, M. Schlesinger and J. Rezek, *J. Electrochem. Soc.*, **119**, 8 (1972).

- (38). M. Schlesinger, *J. Electrochem. Soc.*, **121**, 5 (1974).
- (39). M. Schlesinger and B. K. W. Baylis, *J. Electrochem. Soc.*, **121**, 11 (1974).
- (40). B. K. W. Baylis, A. Busuttill, N. E. Hedgecock and M. Schlesinger, *J. Electrochem. Soc.*, **123**, 3 (1976).
- (41). B. K. W. Baylis, N. E. Hedgecock and M. Schlesinger, *J. Electrochem. Soc.*, **124**, 3 (1977).
- (42). B. K. W. Baylis, C. Huang and M. Schlesinger, *J. Electrochem. Soc.*, **126**, 3 (1979).
- (43). J. O. Besenhard and U. Krebber, *J. Electrochem. Soc.*, **136**, 12 (1989).
- (44). R. L. Cohen and K. W. West, *J. Electrochem. Soc.*, **120**, 4 (1973).
- (45). R. L. Meek, *J. Electrochem. Soc.*, **122**, 11 (1975).
- (46). B. K. W. Baylis, A. Busuttill, N. E. Hedgecock and M. Schlesinger, *J. Electrochem. Soc.*, **123**, 9 (1976).
- (47). N. Feldstein, M. Schlesinger, N. E. Hedgecock and S. L. Chow, *J. Electrochem. Soc.*, **121**, 6 (1974).
- (48). S. S. John, D. Lee, I. Dutta and A. Angelopoulos, *J. Electrochem. Soc.*, **157**, 8 (2010).
- (49). T. Osaka, H. Nagasaka and F. Goto, *J. Electrochem. Soc.*, **127**, 11 (1980).
- (50). T. M. Tam, *J. Electrochem. Soc.*, **132**, 5 (1985).
- (51). M. García-Gabaldón, V. Pérez-Herranz, J. García-Antón and J. L. Guiñón, *J. Appl. Electrochem.*, **37** (2007).
- (52). T. Osaka, H. Takematsu and K. Nihei, *J. Electrochem. Soc.*, **127**, 5 (1980).
- (53). S. L. Chow, N. E. Hedgecock and M. Schlesinger, *J. Appl. Electrochem.*, **119**, 12 (1972).
- (54). N. E. Hedgecock, P. Tung and M. Schlesinger, *J. Electrochem. Soc.*, **122**, 7 (1975).
- (55). I. G. Casella and M. Contursi, *Journal of Electroanalytical Chemistry.*, **588** (2006).
- (56). D. Zabetakis and W. J. Dressick, *ACS Applied Materials & Interfaces.*, **1**, 1 (2009).
- (57). S. S. John, I. Dutta and A. P. Angelopoulos, *J. Phys. Chem. C.*, **114**, 32 (2010).

- (58). N. Fritz, H. Koo, Z. Wilson, E. Uzunlar, Z. Wen, X. Yeow, S. A. B. Allen and P. A. Kohl, *J. Electrochem. Soc.*, **159**, 6 (2012).
- (59). Y. Ma and Q. Zhang, *Applied Surface Science.*, **258** (2012).
- (60). Y. Kobayashi and Y. Ishii, *Journal of Nanoparticles.*, (2013).

III. SPECTROPHOTOMETRIC METHOD FOR ANALYZING TIN(II) BY REDOX REACTION USING 3,3',5,5'-TETRAMETHYLBENZIDINE DIHYDROCHLORIDE AND N-BROMOSUCCINIMIDE

A. INTRODUCTION

Tin(II) compounds are important in ^{99m}Tc radiopharmaceutical kits as a stabilizing agent [1], in dental gels and food as a preservative [2-4], and in electroless plating as an electrochemical catalyst [5-8]. For example, the concentration of tin(II) in ^{99m}Tc radiopharmaceutical kits is an important fact of the product's quality, which has to be close to $20\mu\text{g/vial}$ (Lenoscint[®]). Common methods to analyze tin(II) are limited by some combination of the range and/or limit of detection, ease of application, reproducibility, and inability to distinguish tin(II) from tin(IV). A need to rapidly quantitate tin(II) concentration in an electroless plating sensitization solution at concentration less than $0.3\mu\text{g/ml}$ to evaluate its effectiveness motivated the development of the present colorimetric approach.

Common methods for determining tin(II) concentration are summarized in Table I. These methods are organized into the following categories based on different analytical principles: electrochemical method [1-4, 9-16], membrane sensor [15], inductively coupled plasma optical emission spectrometry (ICP-OES) [16], flame atomic absorption spectrometry (FAAS) [17], fluorescence [18] and spectrophotometric methods [19-26]. The electrochemical method, which includes anodic stripping voltammetry (ASV) method [1-4, 9] and differential pulse polarography (DPP) method [10-14], has been widely used because of its selective determination of tin(II) in the presence of tin(IV). The ASV method has a low limit of detection (LOD). For example, an LOD equal to $0.00026\mu\text{g/ml}$ has been determined by Hutton et.al using the ASV method with a Bismuth Film Electrode (BiFE) [3]. However, the limitation of the ASV method

is that it requires either formation of a tin(II) complex such as a tin(II)-oxine complex [1], a tin(II)-tropolone complex [2], or using a modified electrode such as an epoxy-carbon electrode and the BiFE [3, 4, 9]. The DPP method does not require a tin(II) complex or a modified electrode but it is limited by the detecting range and the LOD. Decristoforo et.al reported a DPP method with an LOD equal to 0.005 $\mu\text{g/ml}$ but the concentration range was from 10 to 15 $\mu\text{g/ml}$ [11]. Similarly, using the DPP method Sebastian et.al quantified tin(II) concentration between concentration range 0 to 10 $\mu\text{g/ml}$ but the LOD was 0.5 $\mu\text{g/ml}$ [12].

Recently published methods based on membrane sensor, inductively coupled plasma, atomic absorption spectroscopy, and fluorescence quenching improved the detection concentration range and the LOD, but the constraints in the methods limit their usage. The tin(II) selective potentiometric membrane sensor method was reported to have a concentration range of 0.013 to 1190 $\mu\text{g/ml}$ and a low LOD of 0.0025 $\mu\text{g/ml}$, but the preparation of the membrane electrode was work-intensive [15]. Inductively coupled plasma optical emission spectrometry (ICP-OES) has been used to quantify trace amounts of tin(II) by separating tin(II) from tin(IV) with a biosorbent. However, the recovery of tin(II) in solution was less than 90% [16]. Cloud point extraction (CPE) followed by flame atomic absorption spectrometry (FAAS) is another method that can quantify tin(II) and tin(IV) in a low concentration range (0.01-1.3 $\mu\text{g/ml}$), but the CPE procedure is complicated (including pH and temperature adjustment, centrifugation, and cooling in an ice bath) [17]. Quenching the fluorescence of carbon Nano-dots (C-dots) by tin(II) was found to be able to detect tin(II) concentrations between 0 to 476 $\mu\text{g/ml}$. However, synthesis of the C-dots with a specific size distribution was difficult to repeat [18].

The spectrophotometric method is widely employed. As illustrated by eight published methods listed in Table I, because of the simplicity of applying the linear correlation between the

absorbance and the different concentrations (Beer-Lambert law) [19-26]. However, existing spectrophotometric methods for detecting tin(II) are limited by various constraints. Reducing iodine monochloride [19] or sodium periodate [22] to iodine and extracting iodine with chloroform is a toxic and not sensitive (LOD=0.20 µg/ml) method. Using complexes of molybdenum [20], FerroZine [21], palladium [23], and rhenium [24] is expensive and these chemicals did not improve the LOD. Synthesized chemical diacetylmonoxime p-hydroxybenzoylhydrazone (DMPHBH) was reported to determine tin(II) concentration from 0.25 to 2.76 µg/ml, but synthesizing DMPHBH was time consuming and the LOD was high (0.242 µg/ml) [25]. A spectrophotometric method showed improvement in both the concentration range and the LOD using the mean centering of ratio kinetic profiles was reported by Madrakian et.al. This method was operated at a concentration range of 0.10 to 1.80 µg/ml and a LOD of 0.03 µg/ml [26]. However, the detection concentration range and the LOD need to be lowered in order to provide sensitivity competitive with the other methods.

Jang and Roper reported a simple, rapid and accurate method for determining Au(I) using 3,3',5,5'-tetramethylbenzidine dihydrochloride (TMB-d) [27]. The absorption coefficient of the reagent was reported at $2.75 \times 10^5 \text{ cm}^{-1} \text{ mol}^{-1} \text{ L}$ [27], that was 3 times higher than iron-FerroZine complex ($5.56 \times 10^4 \text{ cm}^{-1} \text{ mol}^{-1} \text{ L}$) [21]. In this paper, a spectrophotometric method using TMB-d as the color indicator assay was developed for quantitative measurement of tin(II) in aqueous solution. Reduction of the fully oxidized TMB-d (diimine) resulted in a measurable, proportional decrease in absorption at 452 nm under selected conditions. A linear correlation between the absorption at 452 nm and the tin(II) concentration was generated in concentration range of 0.049 to 0.340 µg/ml. The LOD in this method was calculated at 0.013 µg/ml (3σ) [1-3]. This new method allowed quantification of tin(II) without use of complexation agent, at a lower LOD

(0.013 $\mu\text{g/ml}$) and concentration range (LOQ = 0.049 to 0.340 $\mu\text{g/ml}$) when compared with the other spectrophotometric methods. To date, the lowest published tin(II) LOD and concentration range with spectrophotometric methods has been 0.03 $\mu\text{g/ml}$ and 0.10 to 1.80 $\mu\text{g/ml}$, respectively [26]. Sensitivity of the method introduced herein is comparable to the ASV method using tin(II) complexes as indicators, which reported an LOD at 0.012 $\mu\text{g/ml}$ and a concentration range from 0.03 to 2.38 $\mu\text{g/ml}$ [1,2]. Moreover, this new method is more sensitive than the novel quenching fluorescent of C-dots method, which reported an LOD at 0.043 $\mu\text{g/ml}$ [18].

Table I. Methods for determine tin(II) overview

Method		Technical details	Detection concentration range	Limit of detection (LOD)	Medium (pH)	ref
Electrochemical method	Anodic stripping voltammetry (ASV)	Tin(II)-8-hydroxyquinoline (oxine) complex	0.03-2.38 $\mu\text{g/ml}$ ^a	0.012 $\mu\text{g/ml}$ ^a	Acetate buffer, 0.01 M, pH=6	1
		Tin(II)-tropolone complex	0.03-2.38 $\mu\text{g/ml}$ ^a	0.012 $\mu\text{g/ml}$ ^a	Acetate buffer, 0.05 M, pH=5.5	2
		Bismuth Film Electrode (BiFE)	0.001-0.1 $\mu\text{g/ml}$	0.00026 $\mu\text{g/ml}$	Acetate buffer, 0.1 M, pH=4.5	3
		BiFE	0.01-0.15 $\mu\text{g/ml}$	0.00026 $\mu\text{g/ml}$	HCl and NH_4Cl , pH~1.4	4
		Epoxy-carbon powder composite-8-hydroxyquinoline composite electrode	0.0006-0.119 $\mu\text{g/ml}$ ^b	5.5×10^{-5} $\mu\text{g/ml}$ ^b	Acetate buffer, 0.1M, pH=5.8	9
	Differential pulse polarography (DPP)	Static mercury drop electrode (SMDE)	10-15 $\mu\text{g/ml}$ ^c	0.005 $\mu\text{g/ml}$ ^c	Methanol and perchloric acid	10
		Dropping mercury electrode (DME)	0-5 $\mu\text{g/ml}$		0.7 M NaF, 0.1	11

					M NaNO ₃ , and 0.1 M HEPES ^e , pH=8.0	
		Hanging Mercury Drop Electrode (HMDE)	0-10 µg/ml ^c	0.5 µg/ml ^c	3 M H ₂ SO ₄ and 3 M HCl	12
		SMDE	2.0-6.0 µg/ml	0.21 µg/ml	3 M H ₂ SO ₄ and 3 M HCl	13
		DME	>0.1309 µg/ml ^b	0.0654 5 µg/ml ^b	0.1 M NaOH and 0.1 M KNO ₃	14
Potentiometric membrane sensor		Polyvinyl chloride (PVC) membrane electrode	0.013- 1190 µg/ml ^b	0.0025 µg/ml ^b	HCl and NaOH, pH=2.0- 8.5	15
Inductively coupled plasma optical emission spectrometry (ICP-OES)		Combine ICP-OES and solid phase extraction	0.0-0.200 µg/ml	0.0007 µg/ml	HCl, pH=2.0	16
Flame Atomic Absorption Spectrometry (FAAS)		Combine FAAS and cloud point extraction (CPE)	0.01-1.3 µg/ml	0.0028 6 µg/ml	NH ₃ /NH ₄ Cl buffer, pH=8.0	17
Quenching fluorescence method		Tin (II) quenches fluorescence of carbon Nano dots	0-476 µg/ml ^d	0.043 µg/ml ^d	Water and pH=8 buffer	18
Spectropho- tometric methods	Iodine, 520 nm	Reduce iodine monochloride (ICl) to iodine	8-80 µg/ml		6 M HCl and Carbon tetrachlori- de	19
	Molybden- um- thiocyanat e complex, 460 nm	Reduce molybdenum(VI) to molybdenum(V) and molybdenum(III)	0.5-5.0 µg/ml		3 M HCl	20
	Iron(II)- FerroZine complex, 562 nm	Reduce iron (III) to iron (II)	0.2-3.2 µg/ml		1-1.5 M HCl	21
	Iodate ion (I ₃ ⁻), 350 nm	Reduce sodium periodate to iodine	0.91-3.33 µg/ml ^f	0.20 µg/ml ^c	Sodium acetate and glacial acetic acid,	22

					pH=2.2-4.7	
	Palladium(II)-tin(II) complex, 410 nm	Complex with palladium chloride	3.33-150 $\mu\text{g/ml}$		1.5 M HCl	23
	Rhenium(V)-SCN complex, 353 nm	Reduce rhenium(VII) to rhenium(IV)	1.6-6.4 $\mu\text{g/ml}$	0.2 $\mu\text{g/ml}$	3 M HCl	24
	Tin(II)-DMPHBH complex, 430 nm	Complex with diacetylmonoxime p-hydroxybenzoylhydrazone (DMPHBH)	0.25-2.76 $\mu\text{g/ml}$	0.242 $\mu\text{g/ml}$	Ascorbic acid, HCl and Cetylpyridinium chloride (CPC)	25
	Pyrocatechol violet (PCV), 550 nm	Rate of complex reaction of tin(II) with PCV	0.10-1.80 $\mu\text{g/ml}$	0.03 $\mu\text{g/ml}$	Acetic acid-acetate buffer, 1.0 M, pH=4.0	26
Note: a. 1 $\mu\text{mol/L}$ equals 0.119 $\mu\text{g/ml}$; b. 1.00×10^{-6} M equals 0.119 $\mu\text{g/ml}$; c. 1 ppm equals 1 $\mu\text{g/ml}$; d. 1 mM equals to 119 $\mu\text{g/ml}$; e. HEPES represents N-2-hydroxyethylpiperazine-N'-2-ethane sulphonic acid; f. The conversion is based on the total amount tin(II) added to the acetate buffer.						

B. EXPERIMENTAL METHOD

Apparatus

The light source was purchased from Avantes with a deuterium lamp (215-500 nm) and a halogen lamp (500-2500 nm) (Avalight-DH-S-BAL, Broomfield, CO, USA). The absorption across the spectral ranges 300 to 750 nm was measured using an USB4000-UV-vis from Ocean Optics (Detector range 200-1100 nm) (Dunedin, FL, USA). A pH meter (ORION model 920A, Manufacturer's reported pH measurement range: -2.00 to 19.99) with a tip (ORION 9156 BNWP, Thermo scientific) was used to measure the pH of the buffers. A BRANSON Sonifier 250 from VWR scientific was used to dissolve the TMB-d and NBS in deionized (DI) water.

Reagents

Sodium hydroxide (NaOH) (99.9%) was purchased from Mallinckrodt. Acetic acid (HAc) (99.7%) was purchased from VWR. 3,3',5,5'-Tetramethylbenzidine dihydrochloride (TMB-d) (98.0%) was purchased from Electron Microscopy Sciences. N-Bromosuccinimide (NBS) (99.0%) was purchased from Alfa Aesar. Anhydrous tin(II) chloride (SnCl_2) (99.99%) was purchased from Sigma-Aldrich. The NBS was recrystallized in 95°C water before it was used. The other chemicals were used as obtained. The details of making up the test assays are listed in supporting information.

Acetate buffer (0.2 M, pH=4.3-4.5): Make 12 ml 0.4 M sodium hydroxide (NaOH), and 20 ml 0.4 M acetic acid solution with sodium hydroxide, pure (99.9%) acetic acid and DI-water. Mix 12 ml 0.4 M NaOH with 12 ml 0.4 M acetic acid for 0.2 M Sodium acetate (NaAc). Dilute the rest 8 ml 0.4 ml acetic acid with 8ml DI-water for 0.2 M acetic acid. Mixing the 24ml NaAc and 16 ml acetic acid for 0.2 M acetate buffer pH=4.3-4.5. TMB-d solution (0.3 mM): Weigh 3.0 mg TMB-d, add DI-water 0.094 mg for 1 ml water, sonicate for 1min, keep under aluminum foil to avoid light. NBS solution (0.3 mM): Weigh 2.0 mg NBS (recrystallized in 95°C water), add DI-water 0.0534 mg for 1 ml water, sonicate for 1 min, keep under aluminum foil to avoid light. Standard tin(II) solution (0.3 mM): Weigh 3.0 mg SnCl_2 , add DDD-water 0.57 mg for 1ml water, sonicate for 1 min, keep under nitrogen. Dilute the 3 mM tin(II) to 0.3 mM, take 1.8 ml DDD-water add 0.2 ml 3.0 mM tin(II) mix well.

Procedure

The spectrum of a 1.9 ml acetate buffer (0.2 M, pH=4.3-4.5) in a 1 cm polystyrene cuvette was measured as a reference. A dark background was subtracted by blocking the light source. In the sample cuvette, 0.05 ml TMB-d (0.3 mM), 0.05 ml NBS (0.3 mM, recrystallized at

95°C DI water) and 0.09 ml Degassed Distilled Deionized (DDD)-water were added one by one in the order listed. The solution was mixed using a pipette draw and release. Finally, 0.01 ml tin(II) 0.3 mM (0.170 µg/ml, in total volume of 2.1ml) solution was added into the cuvette and the solution was mixed again using the pipette. The light source was blocked for 3min by switching it off before the absorption data was recorded (TMB-d and NBS are sensitive to light). A detecting concentration range of 0.049 (the LOQ) to 0.340 µg/ml was achieved by adding a different amount of 0.3 mM tin(II) into a constant volume (2.1 ml) of the assay. The standard correlation curve was generated by repeating 7 individual tests (n=7). In each individual test 7 different results (because of signal noise) were recorded by computer in 7 sec. Measured absorption at 452 nm for each sample was normalized to the absorption value at 452 nm in 0 µg/ml tin(II) in each individual test. For example, Figure I shows the absorption spectra of different tin(II) concentration in one standard test. The absorption unit (A.U.) in Figure I was normalized to the highest absorption at 452nm in 0 µg/ml (1.0 A.U.).

Detailed procedures to make the standard correlation curve and to justify the method are described as following. In total, seven experiments repeated the standard correlation curve. The first 3 experiments used 50 µl TMB-d mixing with 50 µl NBS to give the 0 point reference. However, because of the weighting error the equal amount of TMB-d and NBS reaction is not possible in reality. When NBS overwhelming the TMB-d, even tiny amount, 2 µl tin(II) 0.3 mM will not give a spectra change, as tin(II) will be oxidized by NBS instead of reducing diimine. Therefore two of the experiments used 60 µl TMB-d mixing with 50 µl NBS, this can ensure there is TMB-d extra but not high enough to show the charge-transfer complex peak at 370 nm. Table II gives the steps of adding solution and taking the absorption spectra. All the spectra data are normalized to the 100µl DDD-water and 0µl tin(II) solution point.

Table II. Procedure for making standard correlation curve

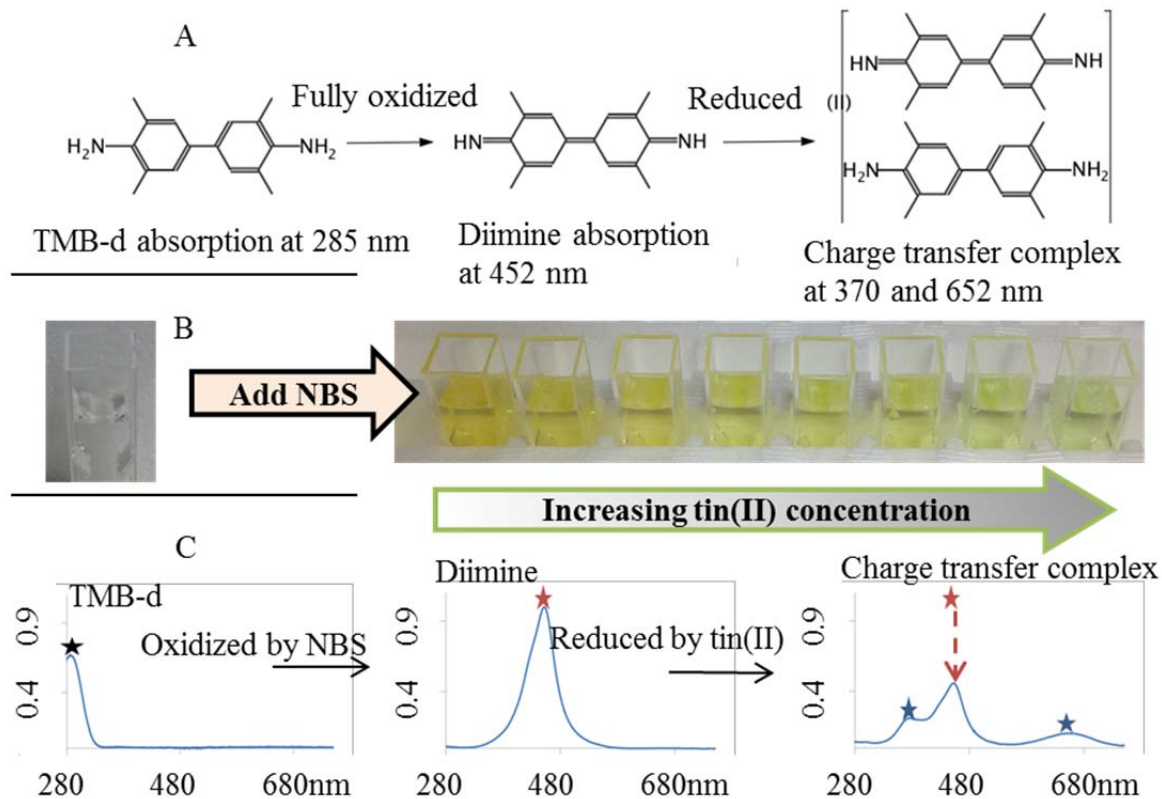
Preparing the solutions and stabilize the light source for half an hour									
Add 1.9 ml acetate buffer into the cuvette, take spectra as reference									
Block the light, take spectra as the dark back ground									
Add TMB-d 0.3 mM solution 50 μ l									
Immediately, add NBS 0.3 mM solution 50 μ l									
Add DDD-water (μ l)	100	98	96	94	92	90	85	80	100
Mix with the pipette, which if for adding DDD-water									
Add 0.3 mM tin(II) (μ l)	0	2	4	6	8	10	15	20	0
Mix with the pipette, which is for adding DDD-water									
Taking 7 spectra every minute, from 0-5 min									
tin(II) concentration convert to (μ g/ml)	0	0.034	0.068	0.102	0.136	0.17	0.255	0.34	0
Absorption data calculated and normalized to the average absorption at 0 point									

C. RESULTS AND DISCUSSION

Mechanism

Using equal moles of NBS and TMB-d to fully oxidize TMB-d to the two-electron oxidation product (diimine) yielded a yellow-brown color solution, which exhibited maximum absorption at 452 nm (Scheme I). The absorption at 452 nm decreased when the concentration of tin(II) increased, because the diimine was reduced to the blue color charge transfer complex form (Scheme I). Based on the difference in redox potential, NBS ($> +1.83$ V, normal hydrogen electrode (NHE)) oxidized TMB-d ($+0.22\sim 0.7$ V, NHE) to diimine [27] and tin(II) ($+0.15$ V,

NHE) reduced the diimine to the charge transfer complex form (Scheme I part A). The yellow color of equimolar TMB-d and NBS mixture (diimine) was reduced to the blue color charge transfer complex form, when the tin(II) solution was added (Scheme I part B, the green color represented a mixture of the diimine and the charge transfer complex form) [27,28]. Meanwhile the tin(II) was oxidized to tin(IV) form. Scheme I part C shows the absorption spectra changed from the initial TMB-d spectra (peak at 285 nm) to the diimine spectra (peak at 452nm), after the TMB-d was fully oxidized by NBS. By adding tin(II) into the diimine a mixture spectra of the charge transfer complex form (two new peaks show at 370 and 652 nm) and the diimine residue (peak at 452 nm) appeared. With increasing tin(II) concentration, more diimine was reduced, thus the solution color was changed from yellow to light yellow to green (Scheme I part B). The spectrophotometer was used to record the absorption spectra change in solution through a 1 cm cuvette, as shown in Figure I. The absorption peak at 452 nm (diimine) decreasing when tin(II) concentration was increased implied that the diimine was reduced by tin(II). On the other hand, the absorption peaks at 370 and 652 nm (the charge transfer complex form) increased with increasing tin(II) concentration, that confirmed the diimine was reduced to the charge-transfer complex form [28].



Scheme I. Tin(II) reducing diimine to charge transfer complex method illustration

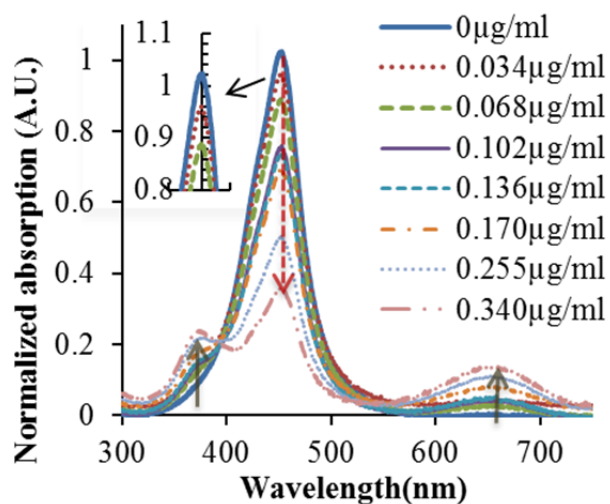


Figure I. Spectra change with increasing tin(II) concentration. (The spectra was recorded 3 min after the reagents were mixed into equimolar TMB-d and NBS buffered to pH 4.4 with acetate.) The red dashed arrow at 452 nm indicates the diimine absorption peak decreased when tin(II) concentration increased. The black solid arrows at 370 and 652 nm showed the charge transfer

complex form absorption peaks increased with increasing tin(II) concentration. The magnitude of the peak intensity change at 452 nm was 3 times higher than at 370 and 652 nm.

Optimum detection condition

Selection of TMB-d/NBS ratio. An equimolar mixture of TMB-d and NBS (50 μ l : 50 μ l in 1.9 ml acetate buffer) displayed the maximum absorption peak height at 452nm. Either increasing or decreasing the relative amount of NBS or TMB-d decreased the corresponding maximum absorption at 452 nm. Figure II red dash line (peak value 0.929), orange solid line (peak value 1.00) and black dot line (peak value 0.873) represent spectra of TMB-d and NBS mixtures at different ratios 50 μ l : 60 μ l, 50 μ l : 50 μ l and 60 μ l : 50 μ l, respectively, normalized to a relative absorption of 1.0. The absorption measured for an equimolar mixture of TMB-d (0.3 mM) and NBS (0.3 mM) (i.e., 50 μ l : 50 μ l in 1.9 ml acetate buffer, pH 4.4 at 25 °C), orange line, was 1.0 absorption units (A.U.) at 452 nm. The absorption peak (452 nm) decreased to 0.929 and 0.873, respectively, when the amount of either NBS (50 μ l : 60 μ l, red line) or TMB-d (60 μ l : 50 μ l, black line) increased. The maximum amount of diimine was produced when the amount of TMB-d and NBS were equal (Figure II orange solid line spectra). Figure II dash red line spectra shows the peak broadened at the bottom (500 nm) that indicated increasing the concentration of NBS caused degradation of the diimine. Meanwhile, Figure II dot black line spectra shows two side peaks appear at 370 and 652 nm that indicated increasing the TMB-d concentration led to the formation of the charge transfer complex form from the diimine and the extra TMB-d.

The added moles of TMB-d and NBS were determined based on the calculated tin(II) monolayer on smooth glass substrates of 0.254 μ g/cm². A substrate with 1×0.5×0.1 cm³ dimension has a surface area of 1.3 cm². The maximum monolayer of tin(II) amount on the substrate is 0.330 μ g and the corresponding concentration in 2.1 ml solution is 0.157 μ g/ml (This

value is just between 0.136 $\mu\text{g/ml}$ and 0.170 $\mu\text{g/ml}$ in the standard correlation curve.). The detection concentration range of the assay could be adjusted by changing the moles of equimolar TMB-d and NBS used in the mixture.

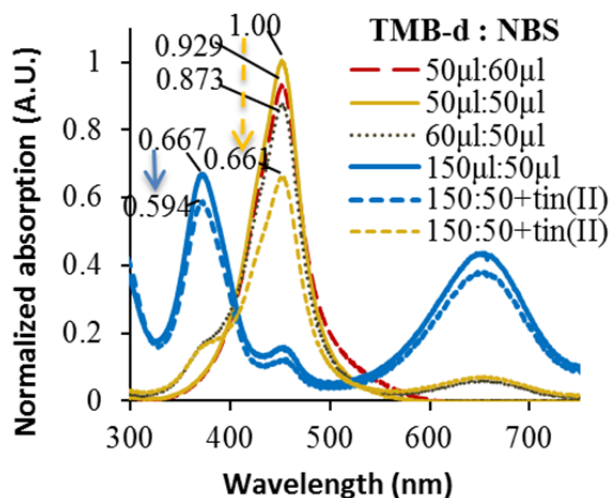


Figure II. TMB-d/NBS ratio and indication peak select. (Spectra were recorded 3 min after the reagents were mixed in pH 4.4 acetate buffer.) The red dash line, orange solid line, black dot line and blue solid line represent TMB-d/NBS ratio of 50 μl : 60 μl , 50 μl : 50 μl , 60 μl : 50 μl and 150 μl : 50 μl , respectively. The orange and blue dashed lines are spectra of TMB-d/NBS ratio of 50 μl : 50 μl and 150 μl : 50 μl with the addition of 10 μl 0.3 mM tin(II) (0.170 $\mu\text{g/ml}$ in total volume), respectively. The orange dash arrow indicates the absorption at 452 nm decreased from 1.00 to 0.661 (A.U.) and blue solid arrow shows the absorption peak at 370 nm decreased from 0.667 to 0.594 (A.U.), when 10 μl 0.3 mM tin(II) (0.170 $\mu\text{g/ml}$ in total volume) was added.

Selection of indicator peak. It was found that the absorption peak at 452 nm (diimine) was 3 times more sensitive to indicating tin(II) than the absorption peak at 370 nm (charge transfer complex form). Figure II, the blue solid arrow shows the total absorption at 370 nm decreased by 0.083 when 10 μl 0.3 mM tin(II), which corresponded to a concentration of 0.170 $\mu\text{g/ml}$ in total volume of 2.1 ml, was added into the mixture of 150 μl 0.3 mM TMB-d and 50 μl 0.3 mM NBS. On the other hand, Figure II brown dash arrow shows the peak at 452 nm (diimine) decreased from 1.00 to 0.661 (by 0.339) when the same amount of tin(II) was added into the mixture of 50 μl 0.3 mM TMB-d and 50 μl 0.3 mM NBS. The absorption decrease at

452 nm (0.339) was 3 times higher than at 370 nm (0.083) that implied the absorption peak at 452 nm was 3 times more sensitive than at 370 nm. Therefore, in this study the diimine absorption peak decrease at 452 nm was employed to quantify the tin(II) concentrations in solution.

Specification of pH using acetate buffer. An acetate buffer (0.2 M) pH between 3.7 and 4.4 at 25 °C generated the optimum absorption at 452 nm (0.976-1.013), after 3min of mixing time. The reaction of NBS oxidizing TMB-d was sensitive to the solution pH value [27,29,30]. In this study, the pH of acetate buffer was adjusted from 2.5 to 5.3. Figure III shows the relation of the acetate buffer pH and the absorption at 452 nm at 25 °C. In a low pH buffer (pH=2.5, 25 °C), the absorption was only 0.370 because the reaction of TMB-d and NBS was inhibited. When the pH value increased to between 3.7 and 4.4 the absorption varied from 0.976 to 1.013. Further increasing the acetate buffer pH to 4.7 the absorption peak dropped to 0.891. The absorption went down to 0.394 when the pH was 5.3, 25 °C. The reason is that at higher pH the diimine degraded and the absorption at 452 nm decreased.

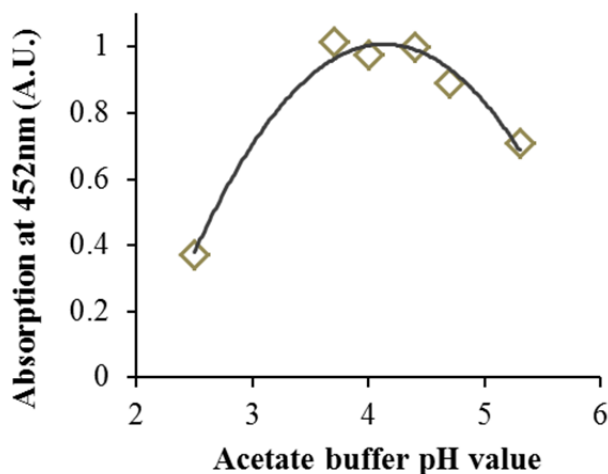


Figure III. Acetate buffer pH effect on absorption. The absorption was recorded after the assays were mixed for 3 min with equal moles of TMB-d and NBS at 452 nm at 25°C.

Mixing time selection. A stable absorption value at 452 nm was obtained by controlling the reaction time for 3 min in pH 4.4 acetate buffer, 25 °C. Figure IV illustrates the reaction time effect on TMB-d redox reaction in different pH acetate. The TMB-d redox reaction rate was increased when buffer's pH value increased. In a buffer with a higher pH than the TMB-d oxidation product, H⁺, is readily scavenged in the buffer, which drives the reaction to the diimine side [28,29]. In a pH equals 2.5 acetate buffer, it took more than 5 min to finish the reaction (Figure IV deep blue diamond). The reaction reached equilibrium at 4 min when the buffer pH increased to 3.7 (Figure IV red box). When the buffer pH was 4.0, the absorption peak value stabilized in less than 2 min (Figure IV green triangle). If the buffer pH was higher than 4.0 (pH=4.4, 4.7 and 5.3), the redox reaction finished immediately after mixing (Figure IV purple, light blue and orange symbols). The absorption-time response was not influenced by the addition of tin(II). Figure V in supporting information shows the absorption at 452 nm change with time before and after adding tin(II) in a pH equals to 4.4 acetate buffer.

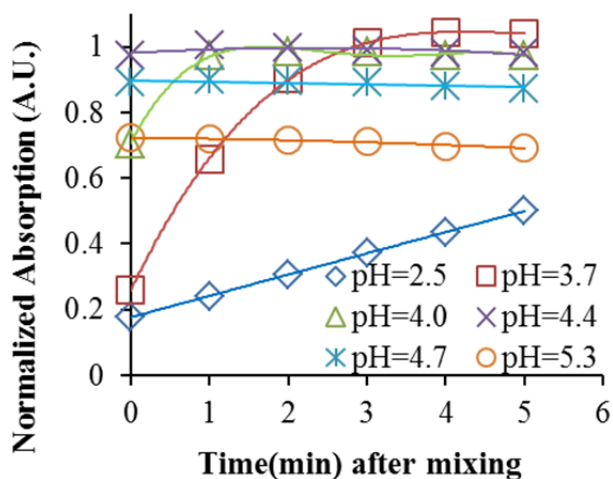


Figure IV. Dynamics of absorption (452 nm) change in acetate buffer with different pH at 25 °C. (Equal moles of TMB-d and NBS were used.) Five different pH conditions are presented, pH=2.5 (♦), pH=3.7 (□), pH=4.0 (△), pH =4.4 (×), pH=4.7 (⋈), pH=5.3 (○).

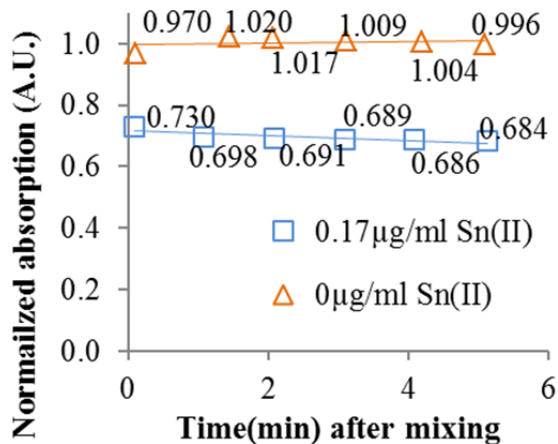


Figure V. Time effect on tin(II) added solution (absorption at 452 nm, pH 4.4 buffer)

Standard correlation curve and error evaluation

Under the optimized condition (Use equal moles of TMB-d and NBS, pH equals 4.4 acetate buffer, record absorption at 452 nm after 3 min reaction), a standard correlation curve of tin(II) concentration and absorption was generated ($R^2=0.9981$, $n=7$) (Figure VI). The diimine absorption peak (452 nm) decrease was correlated to the tin(II) concentration, because it was proved 3 times more sensitive than the charge transfer complex form absorption peaks. In this study, the standard correlation curve was based on 7 repeated tests ($n=7$). In each individual test 7 different data points were recorded for including the instrument error in 7 sec (because of signal-to-noise effects). All the measured values of absolute absorption were normalized so that the absorption of 0 µg/ml tin(II) concentration at 452 nm in each experiment was equal to 1.0 relative absorption units. The error evaluation on y-axis was based on the 7 repeating tests and the 7 continuously data points in each test, which included the method error, the operation error and the system noise. The error evaluation on x-axis was estimated from weighing error and tin(II) oxidation in air, the last digit of the scale (0.1 mg) had a difference of ± 0.05 mg. In experiment 2.0 mg was weighed, the variation was evaluated in 2.0 (± 0.05) mg. Therefore 2.5% of standard deviation error bar was introduced in the standard correlation curve (Figure VI). The

0 $\mu\text{g/ml}$ tin(II) point absorption was repeated at least twice in each test. The standard deviation (σ) at 0 $\mu\text{g/ml}$ tin(II) was determined at 0.0098 (A.U.) and the corresponding limit of detection (LOD) was calculated (3σ) to be 0.013 $\mu\text{g/ml}$. The limit of quantification (LOQ) was calculated (10σ) to be 0.049 $\mu\text{g/ml}$.

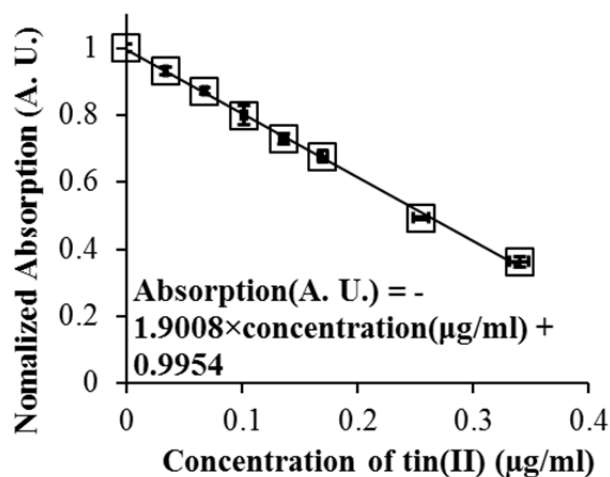


Figure VI. Standard correlation curve of tin(II) concentration and absorption (A.U.). (The absorption values were recorded after the assays were mixed for 3min in pH equals 4.4 acetate buffer with equal moles of TMB-d and NBS at 452 nm.)

Evaluation of Method

This method was evaluated in duplicate by spiking different amounts of 0.3 mM SnCl_2 solution (1, 5, 9, 11, 15 and 19 μl) into 1.9 ml pH 4.4 acetate buffer (25 $^\circ\text{C}$) with equimolar of TMB-d and NBS (0.3 mM) mixture. The absorption correlated with the real concentration was plotted along with the standard correlation curve in Figure VII. A tested concentration result was calculated based on the obtained absorption and the standard correlation curve in Figure V. Table III lists all the tested concentration results of the two tests and the real tin(II) concentrations injected. The deviations of the tested results from the real concentrations were calculated and varied from 0.014 to 0.042 $\mu\text{g/ml}$ at different concentrations. The maximum deviation was 0.042 $\mu\text{g/ml}$ at tin(II) concentration of 0.255 $\mu\text{g/ml}$ and the minimum deviation was 0.014 $\mu\text{g/ml}$ at

0.017 µg/ml. The deviation was hypothesized to come from the standard tin(II) concentration difference and deviation in measurement method used for this component.

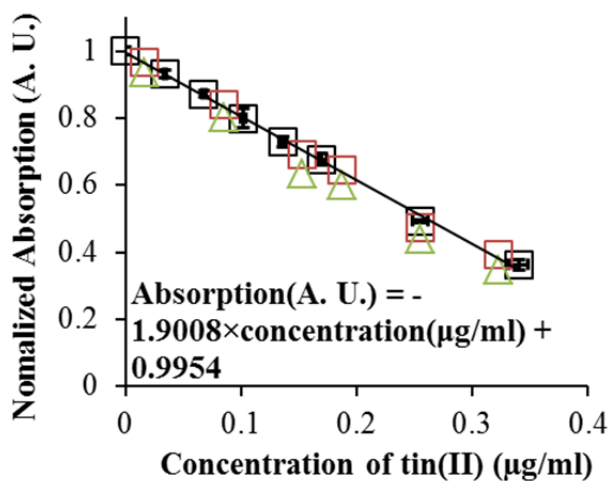


Figure VII. Tested points plotted on the standard correlation curve (red square represents test 1 and green triangle represents test 2).

Table III. Method test with different amount of 0.3 mM tin(II)

Test amount of 0.3mM tin(II) (µl)	1	11	5	15	9	19
Real tin(II) concentration (µg/ml)	0.017	0.187	0.085	0.255	0.153	0.323
Test 1. Absorption (A.U.)	0.967	0.645	0.841	0.473	0.692	0.391
Test 1. Calculated concentration (µg/ml)	0.015	0.184	0.081	0.275	0.160	0.318
Test 2. Absorption (A.U.)	0.937	0.600	0.800	0.439	0.635	0.350
Test 2. Calculated concentration (µg/ml)	0.031	0.208	0.103	0.293	0.190	0.342
Deviation from the real value (µg/ml)	0.014	0.021	0.018	0.042	0.037	0.019

D. CONCLUSIONS

A linear correlation curve of tin(II) concentration and absorption ($R^2=0.9981$, $n=7$) in concentration range from 0.049 (LOQ) to 0.340 $\mu\text{g/ml}$ was obtained by using 3,3',5,5'-tetramethylbenzidine dihydrochloride (TMB-d) and N-bromosuccinimide (NBS) mixture as a spectra indicator. The detection conditions were optimized to obtain intensive, fast, and stable absorption at 452 nm. An equimolar mixture of TMB-d and NBS at 0.3 mM exhibited the maximum absorption at 452 nm. The 452 nm peak (diimine) was selected for detection because it was 3 times more sensitive than the peak at 370 nm (charge transfer complex form) or the peak at 652 nm. The pH of the acetate buffer and the reaction time were optimized to pH 4.4 at 25 °C and 3 min, respectively. A lower range of detection (0.049 to 0.340 $\mu\text{g/ml}$) was obtained in this method when compared with the other spectrophotometric methods [19-26] (Table I). Meanwhile the LOD was improved to 0.013 $\mu\text{g/ml}$ from a recently published spectrophotometric method value of 0.03 $\mu\text{g/ml}$ [26]. The simplicity and sensitivity of this spectrophotometric method make it preferable to the other published methods.

E. REFERENCES

- (1). Boutakhrit, K.; Yang, Z.; Kauffmann, J. *Talanta* **1995**, *42*, 1883-1890.
- (2). Boutakhrit, K.; Quarin, G.; Özkan, S.; Kauffmann, J. *Electroanalysis* **1996**, *8*, 789-794.
- (3). Hutton, E. A.; Hočevár, S. B.; Mauko, L.; Ogorevc, B. *Anal. Chim. Acta* **2006**, *580*, 244-250.
- (4). Jiang, X.; Sun, Q.; Zhang, J.; Wang, B.; Du, X. *Sensor Letters* **2009**, *7*, 97-101.
- (5). Menon, V. P.; Martin, C. R. *Anal. Chem.* **1995**, *67*, 1920-1928.
- (6). Ahn, W.; Taylor, B.; Dall'Asén, A. G.; Roper, D. K. *Langmuir* **2008**, *24*, 4174-4184.
- (7). Jang, G.; Roper, D. K. *The Journal of Physical Chemistry C* **2009**, *113*, 19228-19236.

- (8). Mallory, G. O.; Hajdu, J. B. *Electroless plating: fundamentals and applications*; Access Online via Elsevier: 1990.
- (9). Khoo, S. B.; Ye, R. *Analyst* **2000**, *125*, 895-902.
- (10). Decristoforo, C.; Obendorf, D.; Reichart, E.; Stubauer, G.; Riccabona, G. *Nucl. Med. Biol.* **1998**, *25*, 675-683.
- (11). Lejeune, R.; Thunus, J.; Thunus, L. *Anal. Chim. Acta* **1996**, *332*, 67-71.
- (12). Sebastian, M. V.; Lugon, M. D. M.; da Silva, J. L.; Fukumori, N. T.; de Pereira, N. P.; da Silva, C. P.; Matsuda, M. M. *International Nuclear Atlantic Conference (INAC)* **2007**.
- (13). Almeida, É. V.; di MV Lugon, M.; da Silva, J. L.; Fukumori, N. T.; de Pereira, N. P.; Matsuda, M. M. *J. Nucl. Med. Technol.* **2011**, *39*, 307-311.
- (14). Unal, U.; Somer, G. *Turk J Chem* **2011**, *35*, 73-85.
- (15). Chandra, S.; Sharma, K.; Kumar, A. *Journal of Chemistry* **2012**, *2013*.
- (16). Caldorin, R.; Menegário, A. A. *Microchimica Acta* **2007**, *157*, 201-207.
- (17). Ulusoy, S.; Ulusoy, H. I.; Akçay, M.; Gürkan, R. *Food Chem.* **2012**, *134*, 419-426.
- (18). Yazid, Siti Nur Akmar Mohd; Chin, S. F.; Pang, S. C.; Ng, S. M. *Microchimica Acta* **2013**, *180*, 137-143.
- (19). Pyare, R.; Nath, P. *Analyst* **1985**, *110*, 1321-1323.
- (20). Doronchenkova, T.; Inkin, A.; Kharlamov, V. *Pharmaceutical Chemistry Journal* **1988**, *22*, 254-258.
- (21). Bajic, S. J.; Jaselskis, B. *Analyst* **1991**, *116*, 1059-1061.
- (22). El-Shahawi, M. S.; Abu Zuhri, A. Z. *Bull. Chem. Soc. Jpn.* **1998**, *71*, 597-601.
- (23). Mushtaq, A.; Haider, I. *Applied radiation and isotopes* **1999**, *50*, 649-653.
- (24). Épshtein, N.; Terekhova, T.; Kharitonov, Y. Y.; Skvortsov, V. *Pharmaceutical Chemistry Journal* **2004**, *38*, 284-286.
- (25). Varghese, A.; Khadar, A. *Acta chimica slovenica* **2006**, *53*, 374.
- (26). Madrakian, T.; Afkhami, A.; Moein, R.; Bahram, M. *Talanta* **2007**, *72*, 1847-1852.
- (27). Jang, G.; Roper, D. K. *Anal. Chem.* **2011**, *83*, 1836-1842.

- (28). Josephy, P. D.; Eling, T.; Mason, R. P. *J. Biol. Chem.* **1982**, *257*, 3669-3675.
- (29). Yang, R.; Wang, K.; Xiao, D.; Luo, K.; Yang, X. *Analyst* **2000**, *125*, 877-882.
- (30). Marquez, L. A.; Dunford, H. B. *Biochemistry* **1997**, *36*, 9349-9355.

IV. TIN(II) CONCENTRATION ON TIN SENSITIZED SODA LIME GLASS

SUBSTRATES

A. INTRODUCTION

Electroless plating has been a cost-effective, versatile method to deposit metal onto ceramic and polymeric substrates [1]. Relative to other metallization methods such as chemical vapor deposition, electroless plating can deposit metal on nonconductive substrates with a range of physicochemistry and morphologies at ambient conditions [2, 3]. This versatility has resulted in broad application. Electroless plating has been used to fabricate electrical interconnects at submicron and nano scales [3]. Electroless plating of silver on polystyrene spheres to form polymer/metal (PS/Ag) composite microspheres found use as fillers in anisotropic conductive films [4]. Electroless plating of gold on glass substrate has been evaluated for use as sensors to measure the dielectric constant of solution [5]. Platinum catalyst formed by electroless plating was found more effective for oxygen reduction reaction [6]. Metal composite membranes fabricated by electroless plating have been used in catalytic membrane reactors [7].

The mechanism of electroless plating has been evaluated in previous reports [8, 9]. In conventional two-step activation process, the stannous ion (Sn^{2+}) is first deposited on the substrates during a tin sensitization step. A following reduction step reduces more noble ions like silver(I) to metals like catalytic silver(0) via an accompanying redox reaction, $\text{Sn}^{2+} + 2\text{Ag}^+ \rightarrow \text{Sn}^{4+} + 2\text{Ag}$. Subsequent exposure to a more noble ion like gold(I) has resulted in galvanic displacement of silver metal by gold(0). This step catalyzed further redox-driven reduction of gold(I) to gold(0). However, there has not been comprehensive, systematic evaluation of effects of tin(II) surface concentration on electroless plating.

Tin sensitization has been an important first step in many electroless plating processes. For this reason, the effectiveness of tin sensitization has been studied by different methods, such as contact angle measurement [10, 11, 12]. The concentration of stannous ion on the substrate after tin sensitization has been quantified by different methods. Radiochemical tracer analysis showed tin(II) concentration was 1.2×10^{16} atoms/cm² on Teflon substrates with stannic and stannous chloride as sensitization solution [13]. Rutherford back scattering analysis showed the total tin concentration was 3.5×10^{15} atoms/cm² on Si₃N₄ substrates with Pd-Sn complex solution activation [14]. X-ray fluorescence spectrometry found the total tin concentration was 0.53 - 0.89×10^{15} atoms/cm² on polycrystalline alumina substrates with stannous chloride solution (pH<1 adjusted by HCl) [15]. Radiochemical tracer analysis and X-ray spectrometry rely on potentially harmful radioactivity while back scattering analysis requires expensive, high-energy apparatus. An inexpensive, less harmful spectroscopic approach could expand understanding of tin sensitization and support real-time, inline evaluation during processing.

This study evaluates quantification of tin(II) concentration on sensitized glass substrates using a spectrophotometric method that employs inexpensive, commercially-available redox reagents. The sensitization time, solution concentration, substrate geometry, and the post expose process were examined as factors that could influence the tin(II) concentration on the substrates. The effect of different tin(II) concentrations on subsequent gold metal island formation upon further galvanic electroless plating was evaluated.

B. EXPERIMENTAL METHOD

Materials

Sodium hydroxide (NaOH) (99.9%) and sodium sulfite anhydrous (Na₂SO₃) (98.6%) were purchased from Mallinckrodt. Acetic acid (HAc) (99.7%) was purchased from VWR.

3,3',5,5'-Tetramethylbenzidine dihydrochloride (TMB-d) (98.0%) and silver nitrate (AgNO_3) were purchased from Electron Microscopy Sciences. N-Bromosuccinimide (NBS) (99.0%) was purchased from Alfa Aesar. Formaldehyde with stabilizer (CH_2O) (36.5-38.0%) was from ScienceLab.com Inc. Anhydrous tin(II) chloride (SnCl_2) (99.99%) was purchased from Sigma-Aldrich. Ammonia solution (NH_4OH) (28.0-30%) and hydrochloric acid (HCl) (36.5-38%) were from EMD Chemicals. The trisodium gold bisulfite ($\text{Na}_3\text{Au}(\text{SO}_3)_2$, Oromerse Part B) was dilute with degased deionized and distilled water 1:2 (Au: water). The soda-lime glass microscope and quartz slides were purchased from VWR. The NBS was recrystallized in 95°C water before it was used. The other chemicals were used as obtained.

Procedure

The soda-lime glass slides were cut into small substrates in 3 sizes for experiment usage. Size A: $0.5 \times 0.5 \times 0.1 \text{ cm}^3$, size B: $1 \times 1 \times 0.1 \text{ cm}^3$, size C: $2.5 \times 0.8 \times 0.1 \text{ cm}^3$. The substrates were all washed with acetone and rinsed with DI-water 3 times, then pretreated in 23% nitric acid (diluted from 70% concentrate nitric acid by DI-water 1:2) for 30 min and washed with DI-water 3 times. All the substrates were immersed in DI-water from more than 24 hours before the sensitization tests. The tin(II)-TFA sensitization solution, silver ammoniac nitrate activation solution and electroless gold plating solution was prepared by the published method [5, 16]. The tin(II)-TFA solution was used in the experiment, unless it was mentioned in the text the tin(II)-HCl solution with the same concentration was used.

The substrate was taken out from the immersing DI-water by tweezers and flushed with DI-water for a few second. The DI-water on the glass substrate was removed by Kim wipe touching the edge of the substrate. The substrate was put in a glass tube and 0.5–1.0 ml of tin(II)-TFA sensitization solution was added into the glass tube. The sensitization was in a nitrogen

environment with Para film sealing and the time was controlled from 20 sec to 5 min. After the tin sensitization step, the substrate was taken out of the glass tube, and then immersed in a beaker with 3-5 ml DDD-water. After the sample was taken out of the DDD-water, remove most of the water on the surface was removed by Kim wipe touching on the edge, then the substrate was again immersed in another 3-5 ml DDD-water.

Quantitative measurement of tin(II) concentration on the substrates followed a spectrophotometric method recently developed in our lab. Briefly, the spectrophotometric method assay was first prepared by adding 1.9 ml acetate buffer (the spectrum was set as reference), 50 μ l TMB-d (0.3 mM), 50 μ l NBS (0.3 mM) and 100 μ l DI-water are added one by one in turn and the solution is mixed by pipette drawing and releasing (an absorption data was recorded as no tin(II) standard (A_0)). The substrate was taken out from the water, then the water on the substrate was removed by Kim wipe touching on the edge of the substrate. After this step, the substrate was immersed into a prepared assay immediately. The assay was mixed with the substrate by pipette drawing and releasing. An absorption data was taken after 2-3 min mixing as sample absorption with tin(II) (A_s). The normalized absorption data was calculated by dividing the with tin(II) absorption by the no tin(II) absorption ($A=A_s/A_0$). According to the standard tin(II) concentration and normalized absorption correlation curve (just submitted result), the tin(II) surface concentration will be evaluated. [17]

The silver activation and gold plating method was performed following published previously published method. The silver activation was in a silver ammoniac nitrate solution for 2 min. The gold plating was in a mixture of 1 part of 1:2 diluted trisodium gold sulfite solution and 6 parts of formaldehyde reducing solution. The gold plating time was controlled at 1 min. The gold nano nucleates sizes and densities were determined by SEM images (Philips XL40, FEI

Hillsboro, OR, USA). UV-vis spectra and microscope image were taken after the processes by a digital camera (Infinity 1-5, Lumenera Corporation, Ottawa, CA) integrated with a microscope (Eclipse LV100, Nikon Instruments, Melville, NY USA) in brightfield transmission mode.

C. RESULTS AND DISCUSSION

Sensitization time effect

The sensitization time was found not affect the amount of tin(II) deposited on the substrates, when the time was between 20 sec and 5 min and the tin(II) concentration was 26 mM. Figure I shows when the tin sensitization decreased from 5 min to 20 sec, the tin(II) concentration on the substrates was not decreasing. The tin(II) concentrations for all the different sensitization times (from 20 sec to 5 min) were between 6×10^{14} atoms/cm² and 9×10^{14} atoms/cm². These data suggest that the sensitization time after 20 sec does not increase surface tin concentration on this substrate. Previously, sensitization times from 40 sec to 10 min on a variety of substrates have been evaluated. For example, Feldstein et al. used 1 min tin sensitization in studying the contact angle of the tin sensitized different substrates and the sensitizer solution improvement using electron microscope [18, 19]; Schlesinger and Kisel used 10 min tin sensitization to study different sensitizer solution, the effect on the catalytic sites and the nucleate sites [20]. Recently Sung et al. applied 40 sec of tin sensitization for electroless copper plating [21]. This range of tin sensitization times suggests the effect incubation time after a short initial period has been minor – an observation consistent with other data. Meek's study reported the total surface tin concentration was increased when the sensitization time was increase from 2 sec to 5 min [22]. However, close inspection of reported data revealed the error bar of the tin concentration at 200 sec was sufficient to support re-interpretation that the trend in tin concentration did not increase after 30 sec [22].

The tin(II) concentration of between 6×10^{14} atoms/cm² and 9×10^{14} atoms/cm² measured by a redox-based spectroscopic method was similar to earlier literature reports. Table I lists total tin and tin(II) with tin(IV) concentration measured by different techniques. Radiochemical tracer analysis found the tin(II) concentration on tin sensitized Teflon substrates was 1.2×10^{16} atoms/cm² and on the pretreated soda-lime glass the total tin concentration was 6.1×10^{14} atoms/cm² [13, 23]. Total tin concentrations of 3.5×10^{15} and 1.5×10^{16} atoms/cm² were determined by Rutherford backscattering spectroscopy on Si₃N₄ and graphite substrates [14, 22]. The concentration difference might be due to the different sensitization method. The former (3.5×10^{15}) used a single-step (Sn-Pd) mixture solution, while the latter (1.5×10^{16}) used a two-step (first SnCl₂, then PdCl₂) sensitization process. X-ray fluorescent spectrometry study showed the total tin concentration was $0.53\text{-}0.89 \times 10^{15}$ atoms/cm² on polycrystalline alumina substrates [15]. The measured total tin concentrations in the above research were higher than the measured tin(II) concentration in our lab, because the tin(II) could be oxidized to tin(IV) that was not measured.

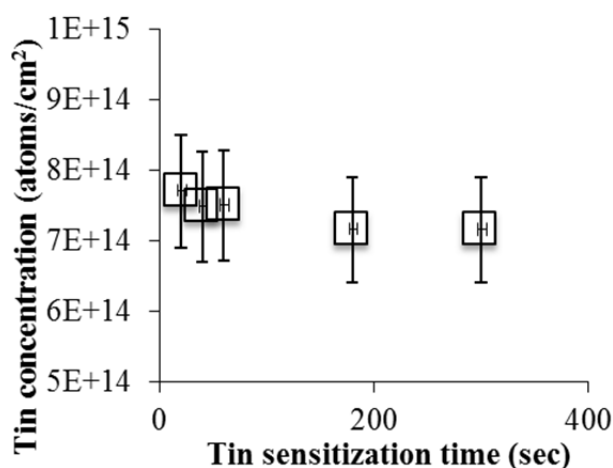


Figure I. Tin(II) concentration on the substrates at different tin sensitization time (x-axis error bar indicated sensitization time varied from -3 to +5 sec, y-axis error bar included the substrates' size error ($\sim \pm 3.7\%$) and the spectrophotometric method error ($\sim \pm 6.7\%$). The tin(II) concentration was at 26 mM tin(II)-TFA solution, the substrate was soda-lime glass 1×1 cm².

Table I. Tin concentration reported by different authors

Ref.	Tin(II) (atoms/cm ²)	Tin(IV) (atoms/cm ²)	Tin (total) (atoms/cm ²)	Methods
13	1.2×10^{16}	0.36×10^{16}	na	Radiochemical tracer
14	na	na	3.5×10^{15}	Rutherford backscattering
15	na	na	$0.53-0.89 \times 10^{15}$	X-ray fluorescent spectrometry
22	na	na	1.5×10^{16}	Rutherford backscattering
23	na	na	6.1×10^{14}	Radiochemical tracer
This work	$0.54-0.93 \times 10^{15}$	na	na	Spectrophotometry

Tin solution concentration effect

The concentration of the tin sensitization solution was found to not have a significant effect on the quantity of the tin(II) finally absorbed on the soda-lime glass substrates after a three minute incubation time, when the tin concentration was decreased from 26 mM to 2.6 mM (TFA concentration was diluted from 72 mM to 7.2 mM). Figure II shows the original tin(II) solution sensitization resulted in an surface tin(II) concentration of between 6×10^{14} atoms/cm² and 9×10^{14} atoms/cm². When the tin(II) solution was diluted to 1:2, 1:4, and 1:9 DDD-water, the tin(II) amount deposited to the substrates kept between 6×10^{14} atoms/cm² and 9×10^{14} atoms/cm². Therefore the concentration had no effect on the tin sensitization, when the concentration was over 2.6 mM. In literature reports, the tin(II) sensitization solution concentrations varied from 0.1 M to 2.5 mM [8, 20, 24, 25]. Schlesinger and Kisel used a mixture solution with 0.1 M SnCl₂ and 0.1M HCl as the basic tin sensitization solution for studying different tin sensitization

solutions [20]. D'Amico et al. used 44 mM SnCl₂ and 0.1 M HCl mixture for tin sensitization [24]. Menon and Martin developed a method for fabricating Nano electrode ensembles by applying the 26 mM tin(II)-TFA solution as the sensitizer [25]. Pederson used a 2.5 mM SnCl₂ with HCl adjust (pH=2.8) solution for surface sensitization in studying the mechanism of electroless plating [8].

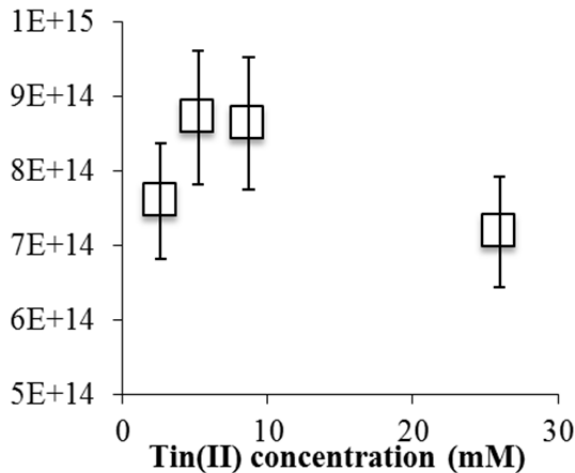


Figure II. Tin(II) concentrations on the substrates at different concentrations of tin sensitization solution (the different tin(II) concentrations were from dilution of the original tin(II) solution). The original tin(II) concentration was at 26 mM and all the sensitization time was at 3 min.

Hydrochloric acid (HCl) and substrates difference

The substrates' size was found not an important fact that would influence the tin(II) concentration on the substrates when the sizes varied from $2.5 \times 0.8 \times 0.1 \text{ cm}^3$ to $0.5 \times 0.5 \times 0.1 \text{ cm}^3$. The surface roughness of the substrates might be an important fact. Although a slight increase of the tin(II) concentration was observed (from below $9 \times 10^{15} \text{ atoms/cm}^2$ to above this value) when the substrate size was decreased from $1 \times 1 \times 0.1 \text{ cm}^3$ to $0.5 \times 0.5 \times 0.1 \text{ cm}^3$ (Figure III), this difference was from the irregular edge increased when the slides was cut smaller. While if the slide size increased to $2.5 \times 0.8 \times 0.1 \text{ cm}^3$, the tin concentration was not changed. Figure IV shows the tin(II) concentration on the quartz substrates is decrease by half to about $3 \times 10^{15} \text{ atoms/cm}^2$. It was possibly the quartz substrates had smoother surface, the actual surface area was lower than

the soda-lime glass even though they had the same sizes. The tin(II)-HCl solution showed the same tin(II) concentration as the tin(II)-TFA solution when the same quartz substrates was tested and the same tin(II) and acid concentration were used.

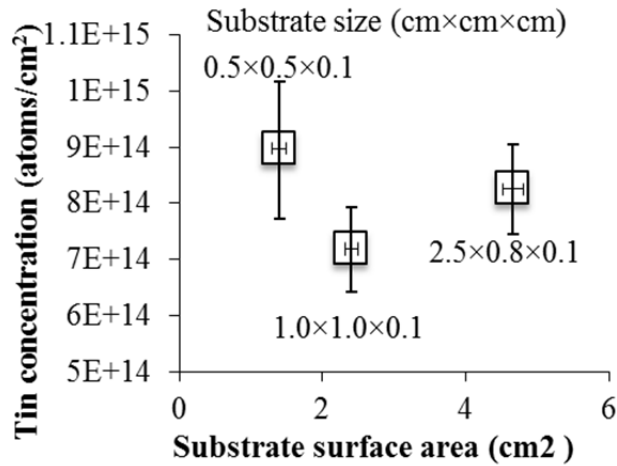


Figure III. Tin(II) concentration on the substrates at different substrate sizes (y-axis error bar included the substrates' size error ($\sim\pm 3.7\%$) and the spectrophotometric method error ($\sim\pm 6.7\%$), and x-axis error bar was only with the size error.). The tin(II) concentration was at 26 mM, and all the sensitization time was at 3 min.

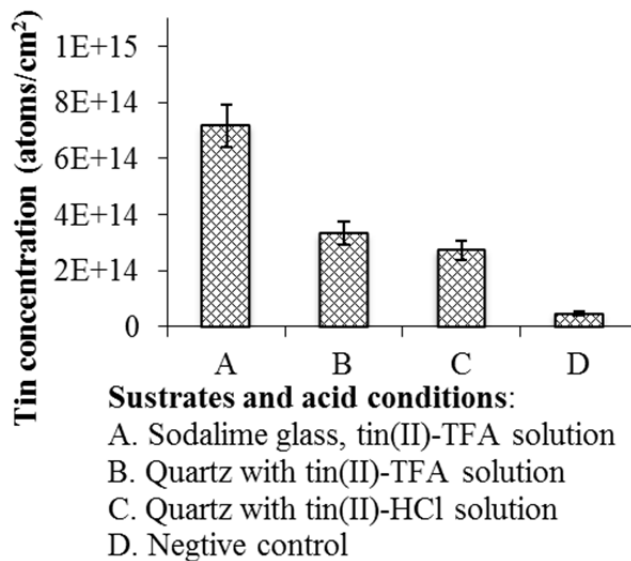


Figure IV. Tin(II) concentration on the soda-lime glass and quartz substrates (error bar included the substrates' size error ($\sim\pm 3.7\%$) and the spectrophotometric method error ($\sim\pm 6.7\%$)). Tin(II)-HCl solution was compared with the tin(II) TFA solution. The negative control was using pretreated soda-lime glass without tin sensitization. The tin(II) concentration was at 26 mM, the acid concentration was at 72 mM, and the sensitization time was kept at 3 min.

Post exposure of the tin sensitized substrates

Water layer absorbed on the substrates was found able to protect the tin(II) layer from being oxidized by the air. After tin sensitization step, 4 different post treatment steps were carried out, keep the substrates in water, with water on the surface naturally dry in air for 20 min, use Kim wipe remove the water on the edge and keep in air for 2 min, and use nitrogen dry the substrates and keep in air for 2 min. Figure V shows the tin(II) concentration difference when the post treatment steps are different. The best way (maximum tin(II) concentration) was keep the substrates in water or with water layer on the substrates and only keep in air for 2 min. If the substrate was dried in air after 20 min the tin(II) concentration would be mostly oxidized in air. If the substrates were dried in nitrogen, only 2 min exposure in air would lead to about 50% decrease in tin(II) concentration on the surface. Therefore, the water layer on the top of the deposited divalent tin(II) layer was critical to avoid the tin(II) being oxidized by the air to tetravalent tin(IV).

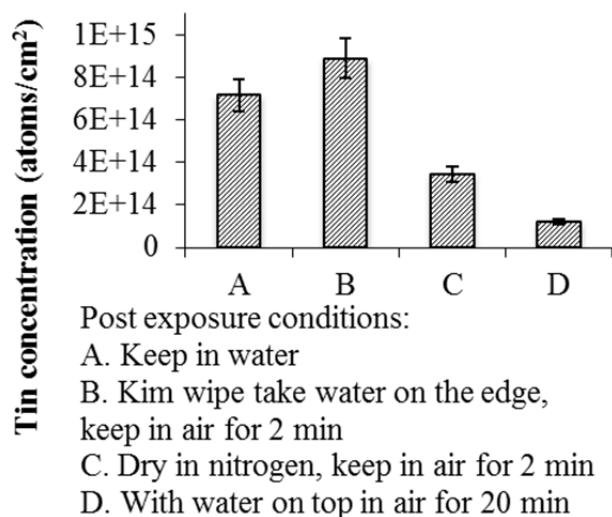


Figure V. Tin(II) concentration on the substrates at different types of post exposure of the substrates (error bar included the substrates' size error ($\sim\pm 3.7\%$) and the spectrophotometric method error ($\sim\pm 6.7\%$)). The negative control was using glass substrates, no tin sensitization, immersing the substrates in the TMB-d and NBS assay. The tin(II) concentration was 26 mM, the acid (TFA and HCl) concentration were at 72 mM, and the sensitization time was at 3 min.

Effect on gold nucleation at the initial stage of electroless gold plating

The initial growing of Au nucleate sites (1 min) on tin sensitized and silver activated substrates was found related to the tin sensitization step (the tin(II) concentration on the substrates). Figure VI show the SEM images of three different tin sensitization processes (A. Keep the substrate in DI water all the time before Ag activation step; B. Use Kim wipe remove most water on the edge of the substrate and keep in air for 2 min; C. Use nitrogen dry the substrate and keep in air for 2 min.) with the same tin(II)-TFA solution, silver activation and gold plating. Table II listed the granule size and density of the gold nucleated on the substrates in different tin sensitization processes. In all the situations the size of the Au particles on the substrates had the same diameter range (15-25 nm). The densities of the Au nucleate sites were accounted based on a $200 \times 200 \text{ nm}^2$ space. Condition A and B showed similar particle density 1250 ± 100 and 1200 ± 100 particles/ μm^2 respectively (Figure VI. A and B), while condition C showed a decrease in particle density to 900 ± 100 particles/ μm^2 (Figure VI. C). The drop of the particle density from 1250 ± 100 to 900 ± 100 particles/ μm^2 was due to the tin(II) concentration dropped from 7.02×10^{14} to 3.47×10^{14} atoms/ cm^2 . It was reported the absorption of the sensitizer, the island density and size changed with using different tin sensitizers [20]. The island sized could vary from 5-6 nm to 75-100 nm when the sensitizer changed from 240 hours aged and 0.05_{wt}% triton X-100 added 0.1 M tin(II)-HCl solution to only 0.05_{wt}% triton X-100 added 0.1 M tin(II)-HCl solution without aging. When the 0.1 M tin(II)-HCl solution aged from 48 to 96 hours the island sized decreased from 29.7 to 11.2 nm after 1 min plating, which had the similar size range of 15-25 nm with the tin(II)-TFA solution (Figure VI). However, the comparison might not convincible, as electroless Ni plating was different with electroless Au plating.

Keeping the tin(II) deposited substrate in water could prevent the tin(II) from oxidation and expose the substrate to air with a water layer covered could possibly prevent the Ag catalytic sites from aggregation. The morphology of the 1 min plated gold film was different in condition A and B, although the total particle density was similar. In condition A, the particles were more aggregated than in condition B (Figure VI. A and B). Meanwhile, in condition C, not only the particle density was lower, but also the particles were aggregated (Figure VI. C). The morphology differences of the different Au films were possibly due to the differences in the Ag activation, which was controlled by the tin sensitization. The catalytic sites were usually less than 10 nm in size, so SEM was not sufficient to take a clear image of the catalytic sites. The UV-vis spectra were used to qualitatively compare the different Ag activation results from different tin sensitization processes. Figure VII shows the extinction of the Ag catalyst deposited glass substrates with clean glass substrate as reference. The extinctions of process A and B were higher than process C, because more tin(II) was found on the substrate (See Table II) and more silver catalytic sites were reduced on to the substrates. However, the extinction of process B was higher than process A was not clear, because process A keep the tin sensitized substrate in water should give the maximum or close to process B (as the result indicated) tin(II) concentration, the Ag catalytic site should be close. Our hypothesis is the Ag catalytic sites in process A was aggregated, as we observed in Figure VI comparing the 1 min gold plated films, case A is much more aggregated than case B. Therefore, keep the tin(II) deposited substrate in air from short time (2 min) while covered with a thin layer of water could possibly prevent the Ag catalytic sites from aggregation. Figure VII shows UV-vis spectra of 1 min gold plated films from three different tin processes. Combining Figure VII with Figure VI the SEM images, process C showed the lowest extinction because less gold particles were on the substrate and the particles

were aggregated. Process B had higher than process A, because the Au particles in B were less aggregated than in A. However, for these gold films no dips at around 500 nm wavelengths which was due to photoluminescence were observed compared with literatures [16, 26].

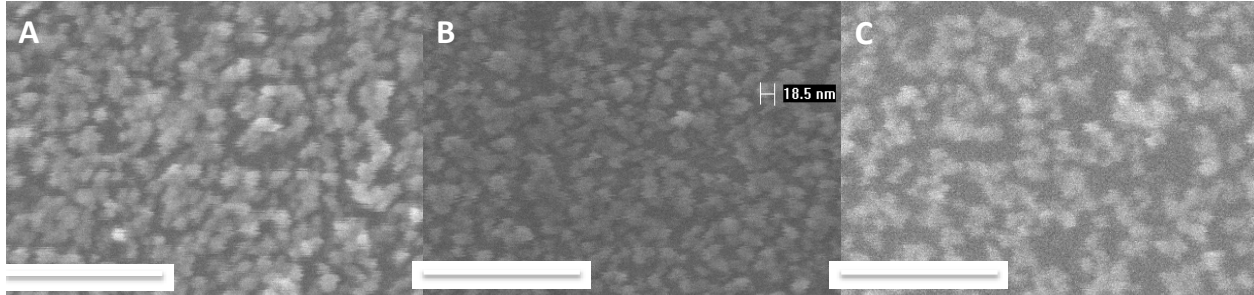


Figure VI. Scanning electron microscopy (SEM) images of 2 min Ag activated and 1 min Au plated soda-lime glass substrates with different post treatment after tin sensitization. (A) Keep the substrate in DI water all the time before Ag activation step. (B) Use Kim wipe remove most water on the edge of the substrate and keep in air for 2 min. (C) Use nitrogen dry the substrate and keep in air for 2 min. (All the scale bars in the images are 200 nm)

Table II. Gold nucleate site concentration and tin(II) concentration

Method	Tin(II) concentration (atoms/cm ²)	Au nucleate size (nm)	Au nucleate site concentration (particles/μm ²)
A. Keep in water	$7.02 \pm 0.75 \times 10^{14}$	15-25	1250 ± 100
B. Kim wipe remove water on the edge and keep in air for 2 min	$8.90 \pm 0.93 \times 10^{14}$ (This was only one test, A and C conditions 4 tests.)	15-25	1200 ± 100
C. Nitrogen dry and keep in air for 2 min	$3.47 \pm 0.36 \times 10^{14}$	15-20	900 ± 100

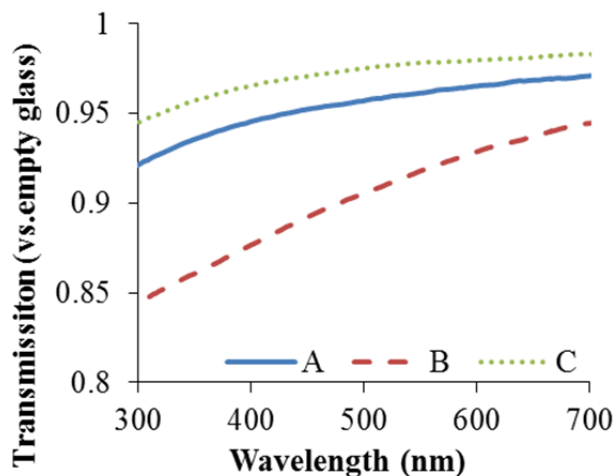


Figure VII. UV-vis spectra of 2 min Ag activated substrates with different tin sensitization processes. The substrate was kept in water after sensitization and washed twice (blue line A), the substrate was taken out of the water and kept in air for 2 min with a thin layer of water on the top before Ag activation (red dash line B), the substrate was dried in nitrogen and kept in air for 2 min before Ag activation (green dot line C).

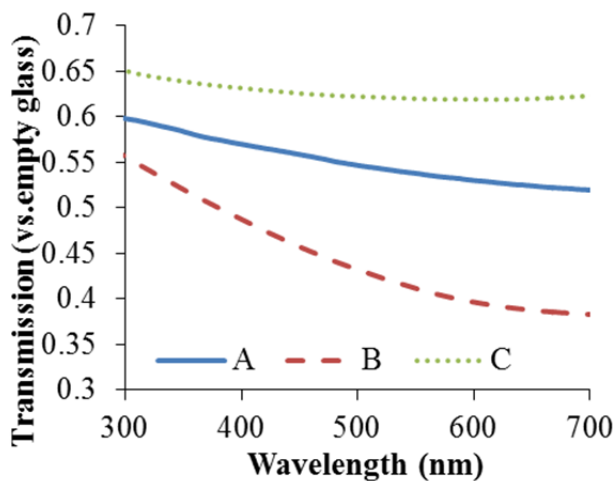


Figure VIII. UV-vis spectra of 1 min Au plated substrates after 2 min Ag activation with different tin sensitization processes. The substrate was kept in water after sensitization and washed twice (blue line A), the substrate was taken out of the water and kept in air for 2 min with a thin layer of water on the top before Ag activation (red dash line B), the substrate was dried in nitrogen and kept in air for 2 min before Ag activation (green dot line C).

D. CONCLUSIONS

The sensitization time, solution concentration, substrate, and post exposure were proposed to important facts that could affect the tin(II) concentration deposited onto the substrates. In this study it was found the sensitization time, the solution concentration and the substrate size were not important factors that could influence the tin(II) deposition, when the sensitization time was between 20 sec and 5 min, the SnCl_2 concentration was between 26 and 2.6 mM, and the substrate size was changed from $2.5 \times 0.8 \times 0.1 \text{ cm}^3$ to $0.5 \times 0.5 \times 0.1 \text{ cm}^3$. While the quartz substrates had less tin(II) deposition than the soda-lime glass substrate, ($2.8\text{-}4.3 \times 10^{14}$ atoms/ cm^2 vs. $5.4\text{-}9.3 \times 10^{14}$ atoms/ cm^2), which might due to the quartz surface was much smooth than the soda-lime glass. Changing the acid condition by switching from 72 mM TFA to 72 mM HCl the tin(II) concentration on the substrates were at the same level (around 2.8×10^{14} atoms/ cm^2).

Post exposure process of the tin(II) sensitized substrate was found the most critical fact that could change the tin(II) concentration. It was found keeping the tin(II) deposited substrate in water could prevent the tin(II) from oxidation by air to tetravalent tin(IV). Even a single water layer on the substrate and the substrate was exposed to the air for 2 min, the tin(II) on the substrate would still be protected by water layer. While about half of the tin(II) was oxidized if the tin(II) deposited substrate was dried in nitrogen and exposed in air for 2 min. UV-vis showed the more the tin(II) concentration on the substrate, a higher extinction value was obtained after both 2 min silver activation and 1 min gold plating. SEM images confirmed the density of the gold islands was determined by the tin(II) concentration on the substrate. The higher the tin(II) concentration the density of the gold island would also be higher. While the gold island size was all the same in different tin(II) concentration conditions.

E. REFERENCES

- (1). N. Fritz, H. Koo, Z. Wilson, E. Uzunlar, Z. Wen, X. Yeow, S. A. B. Allen and P. A. Kohl, *J. Electrochem. Soc.*, **159**, 6 (2012).
- (2). K. G. Mishra and R. K. Paramguru, *African Journal of Pure and Applied Chemistry.*, **4**, 6 (2010).
- (3). D. Zabetakis and W. J. Dressick, *ACS Applied Materials & Interfaces.*, **1**, 1 (2009).
- (4). Y. Ma and Q. Zhang, *Applied Surface Science.*, **258** (2012).
- (5). Y. Kobayashi and Y. Ishii, *Journal of Nanoparticles.*, (2013).
- (6). S. S. John, I. Dutta and A. P. Angelopoulos, *J. Phys. Chem. C.*, **114**, 32 (2010).
- (7). M. Volpe, R. Inguanta, S. Piazza and C. Sunseri, *Surface & Coatings Technology.*, **200**, (2006).
- (8). L. R. Pederson, *Solar Energy Materials.*, **6**, 2 (1982).
- (9). G. Jang, M. E. Hawkrige and D. K. Roper, *J. Mater. Chem.*, **22** (2012).
- (10). N. Feldstein, J. A. Weiner and G. L. Schnable, *J. Electrochem. Soc.*, **119**, 11 (1972).
- (11). H. Koo, S. Y. Kim, S. K. Cho and J. J. Kim, *J. Electrochem. Soc.*, **155**, 9 (2008).
- (12). N. Feldstein and J. A. Weiner, *J. Electrochem. Soc.*, **119**, 6 (1972).
- (13). N. Feldstein and J. A. Weiner, *J. Electrochem. Soc.*, **120**, 4 (1973).
- (14). M. Froment, E. Queau, J. R. Martin and G. Stremmsdoerfer, *J. Electrochem. Soc.*, **142**, 10 (1995).
- (15). J. W. Severin, R. Hokke, H. van der Wel and G. de With, *J. Electrochem. Soc.*, **140**, 3 (1993).
- (16). W. Ahn, B. Taylor, A. G. Dall'Asen and D. K. Roper, *Langmuir.*, **24**, 8 (2008).
- (17). X. Wei and D. K. Roper, *Journal of Analytical Chemistry* just submitted.
- (18). N. Feldstein and J. A. Weiner, *J. Electrochem. Soc.*, **119**, 6 (1972).
- (19). N. Feldstein, S. L. Chow and M. Schlesinger, *J. Electrochem. Soc.*, **120**, 7 (1973).
- (20). M. Schlesinger and J. Kisel, *J. Electrochem. Soc.*, **136**, 6 (1989).

- (21). Y. Sung, C. Lai, S. Lin and Chang Shou-Yi, *Electrochemical and Solid-State Letters.*, **9**, 5 (2006).
- (22). R. L. Meek, *J. Electrochem. Soc.*, **122**, 11 (1975).
- (23). C. H. de Minjer and v.d. Boom, P. F. J., *J. Electrochem. Soc.*, **120**, 12 (1973).
- (24). J. F. D'Amico, M. A. De Angelo, J. F. Henrickson, J. T. Kenney and D. J. Sharp, *J. Electrochem. Soc.*, **118**, 10 (1971).
- (25). V. P. Menon and C. R. Martin, *Anal. Chem.*, **67**, 13 (1995).
- (26). G. Jang and D. K. Roper, *J. Phys. Chem. C.*, **113**, 44 (2009).

V. ELECTROLESS GOLD PLATING FOR 2D HEXAGONAL ARRAYS OF NANO RINGS AND 3D NANOSTRUCTURES GROWTH

A. INTRODUCTION

The metallic rings had potential applications in chemical and biological sensing (surface enhanced Raman scattering (SERS), surface-enhanced infrared absorption and localized surface plasmon resonance (LSPR) sensing), optical telecommunications, optical data storage, and enhancing photoluminescence signals [6]. Different methods of fabricating metallic rings were reported. Gold and silver rings on silicone substrate, which had potential usage in SERS, were fabricated by edge spreading lithography (ESL) with silica beads [1]. SERS on square arrays of gold nano holes and nano disks fabricated by electron beam lithography (EBL) were studied [3]. Interference lithography and thermal annealing of the colloidal gold nano particles fabricated large area square arrays of gold nano rings with adjustable sizes and shapes [8]. Gold rings with diameters of 100-500 nm were fabricated by using silica colloids particle imprinted templates [10].

Babayan et al. reported metallic ring structures as a tool for confining light into a corral [5]. It was found that the ratio of the ring thickness to the ring diameter was critical for plasmon resonance [5]. The Discrete Dipole Approximation (DDA) study of the square array gold nano cylinders found the LSPR peak was related to the height, diameter, roughness, and thickness of the chromium adhesion layer [2]. When the diameter of the cylinder was 90 nm, the LSPR peak shifted from 700 nm to 600 nm if the height of the cylinder increased from 20 nm to 60 nm. If the height of the cylinder was constant, the LSPR peak red shifted if the diameter of the cylinder increased from 50 nm to 200 nm. Meanwhile, the roughness of the cylinder induced a red shift [2]. At a constant edge-to-edge distance, when the diameter increased, the Raman scattering

enhancement increased for nano holes, but decreased for nano disks [3]. SERS in gold nano rings (with inner and outer diameters of 60 and 100 nm) and ring dimers were compared to the SERS in disk dimers; the peak field enhancement for ring dimers was found to be higher than the disk dimers [4]. Gold nano rings fabricated by colloidal lithography with radii of ~60 nm showed that the surface plasmon resonances (SPR) wavelength could be tuned by the wall thickness [7].

Meanwhile, parabola-shaped subwavelength structures showed a broad low reflectance in the range of 300-2000 nm at 7.80% (average value), which had potential application in optoelectronic devices [11]. Another study showed parabola-shaped periodic subwavelength grating structures on aluminum-doped zinc oxide film/Si substrate showed a low average reflectance of ~5% in the wavelength range of 300-1100 nm [12]. Ag and Al nano spheroids deposited on the top of the solar cell could enhance the optical absorption of the cell [13]. Gold films with nano-sized holes exhibited a LSPR in the red to near-infrared region by elastic scattering measurements [9]. A silver surface with hexagonal arrays of dots (300 nm periodicity) was found to prohibit the light propagation in all directions for modes with energies between 1.91 and 2.00 eV [14].

In this study, the 2D hexagonal arrays of gold nano rings were fabricated by coupling EBL and electroless plating. The optical and thermal properties (green laser heating the substrate) were studied by lifting off gold film with hexagonal gold nanostructures on scotch tape. The 3D gold nano rings and hollow structures were grown based on the 2D gold nano rings. The dynamics of the growing was discussed and the particle sizes changing with growing time were recorded. Potential usage of such gold nanostructures could be in sensors (SERS, LSPR), solar cells and light harvesting materials.

B. METHODS

The 2D gold nano ring structure was fabricated as illustrated in Figure I. First, a 150 nm ZEP 520 (Nippon Zeon Ltd.) was coated on an indium tin oxide (ITO) glass. Second, hexagonal arrays of dots were created by electron beam on the ZEP. The patterns were developed in an amyl acetate solution. Gold was deposited on the substrate by electroless gold plating, following the method used by Ahn and Roper [15]. The substrate with ZEP coated and hexagonal nano dots patterned was immersed in a tin sensitization solution for 3 min (26 mM SnCl_2 and 72 mM CF_3COOH), washed with degassed deionized distilled (DDD)-water, immersed in a silver ammoniac nitrate solution (pH~14) for 2 min, washed again in DDD-water, immersed in a electroless gold plating solution trisodium gold sulfite (Oromerse Part B) with formaldehyde as the reducing agent for 5 min. After the gold film was deposited on the substrate, it was washed again in DI-water and gently dried in nitrogen. The top gold layer and the middle gold array were removed by putting a transparent scotch tape on the top of the gold film and lifting it off. The 2D hexagonal arrays of gold nano rings were left on the ITO substrate. The 3D gold nano rings and hollow structures were fabricated by immersing the 2D gold nano rings in to a electroless gold plating solution with formaldehyde as the reducing agent for different times.

The EBL and gold nanostructures SEM images were taken on Philips XL40 (FEI Hillsboro, OR, USA). The method of developing gold nano dots patterns were following the method reported by Blake et al [16]. UV-vis spectra and microscope images were taken by a digital camera (Infinity 1-5, Lumenera Corporation, Ottawa, CA), which integrated with a microscope (Eclipse LV100, Nikon Instruments, Melville, NY USA) in bright field transmission mode. The reflection, transmission and attenuation were determined by a system consisting of an polytetrafluoroethylene (PTFE) integrating sphere (IS200-4, Thorlabs, Newton, NJ), a 2 mm

diameter resonant laser (MXL-FN-532, CNI, Changchung, CN), a fiber-coupled spectrophotometer (AvaSpec-2048, Avantes, Broomfield, CO. USA), and a power meter (PM100D, Thorlabs, Newton, NJ, USA) [17]. The thermal properties of the substrates were measured on a previously reported system [18-20]. The sample was irradiated with a green laser (MXL-FN-532, CNI, Changchung, CN) at different powers. The temperatures on the substrates were measured by a thermal camera (ICI 7320, Infrared Cameras Inc., Beaumont, TX, USA).

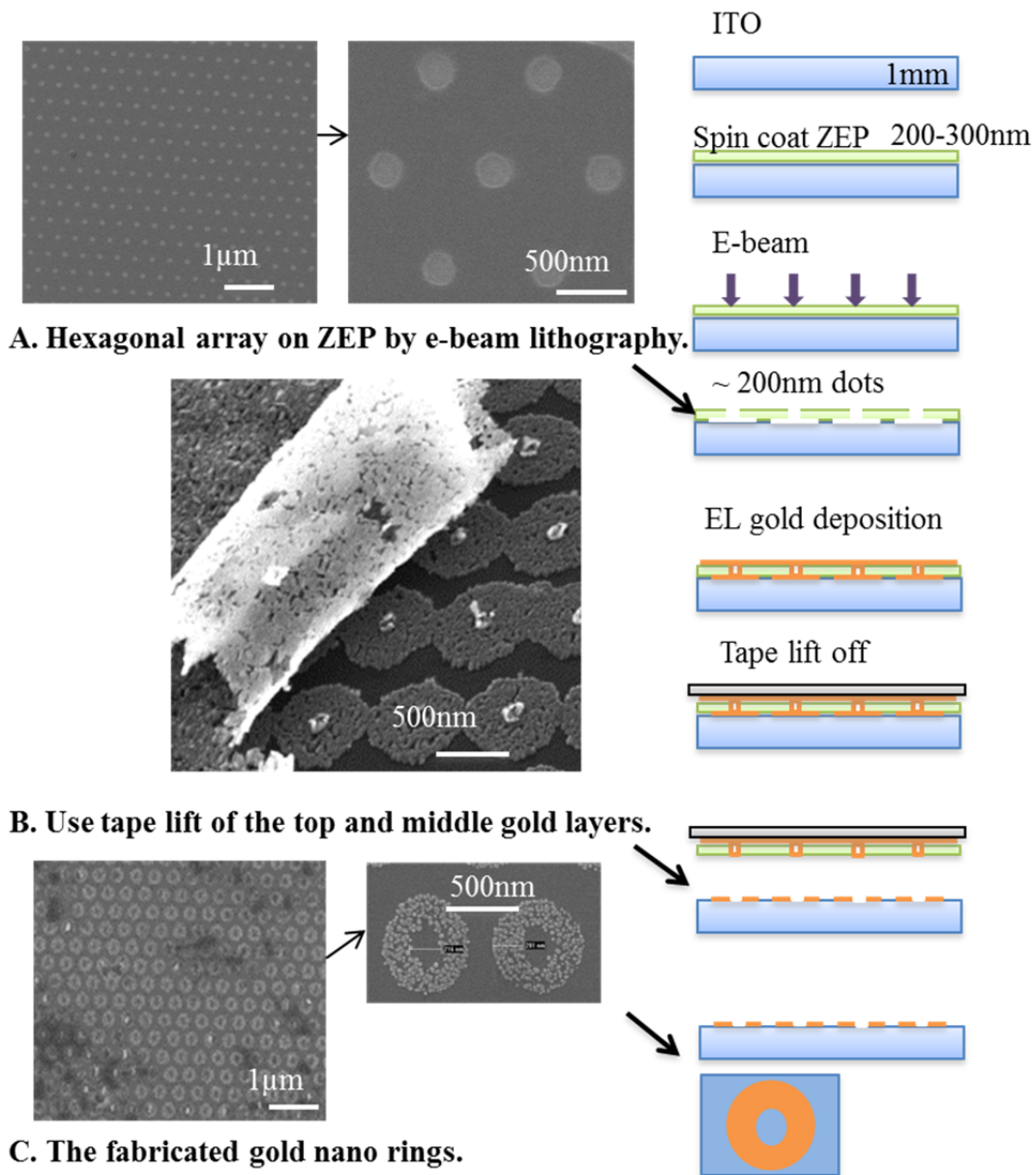


Figure I. Method of 2D gold nano ring fabrication. SEM image A shows the hexagonal arrays of nano dot on ZEP coated ITO glass. Image B shows the top gold film with the middle gold arrays are lifted off by the tape (some gold arrays in the middle are not successfully removed). Image C shows the gold rings in 2D geometry are fabricated. The scheme beside the SEM images indicates the whole process for making the nano rings.

C. RESULTS AND DISCUSSION

After the gold film was lifted off from the ITO glass, two substrates were fabricated: the bottom 2D gold nano rings (Figure I, C) and the top gold film with hexagonal gold nanostructures (Figure II). The bottom 2D gold nano rings and the top gold nanostructures were studied separately by taking SEM images, UV-vis spectra, attenuation, reflection and transmission measurements, and thermal response.

Gold film, ordered array of gold structures and top layer of gold film on the tape

The gold film with hexagonal arrays of structures on top of a scotch tape substrate showed a high efficiency of light to heat conversion ($1267\text{ }^{\circ}\text{C}/\text{W}$). SEM measured the geometry of the hexagonal gold nanostructures (the height was measured by tilting the substrate). The cylinder-shaped hexagonal arrays of gold nanostructures were distributed in a 650-730 nm period. The height of the cylinder-like shape was 120-160 nm, and the thickness was 100-120 nm. The overall size of the arrays was $5\times 5\text{ mm}^2$. Figure II shows the SEM image of the hexagonal gold nanostructures on the gold film that is attached to plastic scotch tape. Thermal response measurement showed the gold film with the hexagonal gold nanostructures had better light-to-heat conversion (in press result). Under the same laser power irradiation (30 mW), the maximum temperature as recorded by thermal camera increased from $22\text{ }^{\circ}\text{C}$ to $50\text{ }^{\circ}\text{C}$ for the gold film on the tape, and from $22\text{ }^{\circ}\text{C}$ to $60\text{ }^{\circ}\text{C}$ for the hexagonal gold array on the gold film; the temperature increase (ΔT) were $28\text{ }^{\circ}\text{C}$ and $38\text{ }^{\circ}\text{C}$ (933 and $1267\text{ }^{\circ}\text{C}/\text{W}$). The hexagonal arrays of gold nanostructures were proved to increase the maximum temperature on the substrate by $10\text{ }^{\circ}\text{C}$.

Similar research of gold nano particle imbedded polydimethylsiloxane (PDMS) membrane showed at a light power loss of 40 mW the temperature increase (ΔT) reached about 30 °C [18]. Other research into gold embedded PDMS membrane showed the ΔT could be improved to 54.5 °C at laser power input of 18 mW [19].

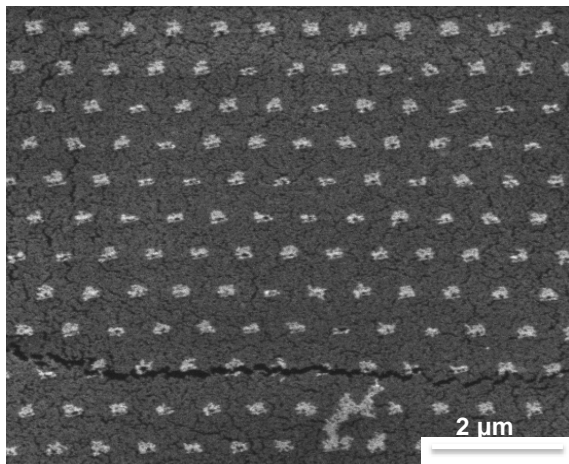


Figure II. SEM images of the hexagonal array the electroless plated Au film with ordered array of nanoparticles

Growing 3D gold nanostructures based on the 2D gold nano rings

Growing of the 3D gold nanostructures. Continuous immersion for 30 min, and 5 min step-by-step immersion of the 2D gold ring structure were studied. Figure III shows the SEM images of initial gold ring in granule structure on a 2D plane (A and B) and the gold hollow structures fabricated by 30 min continuous growth in a gold electroless plating solution (C and D). The original gold ring had an inner diameter of ~200 nm, an outer diameter of ~550 nm, granule size 20-30 nm, and height ~30 nm (Table I). After 30 min immersion in a gold electroless plating solution, the ring developed into a hollow structure 750 nm in size, 250-300 nm in height. The granule sizes ranged between 80 and 200 nm. The mechanism of 3D gold nanostructures growth could be the silver catalyst residue on the gold granule particles, which kept catalyzing the gold(I) ion to gold(0) in a formaldehyde reducing environment. The silver

residue in the gold film by this electroless plating method was detected by X-ray photo spectroscopy (XPS) [21].

Step-by-step growing of 3D gold nanostructures base on the initial gold nano rings was shown by SEM images in Figure IV. Table I lists all the geometries of the rings in different steps. The 2D gold nano ring in step-by-step growing was found to be different from that created by continuous growth. After the first 5 min immersion in gold electroless plating solution, the ring was increased in both size and height, because the granule size was grown from 20-30 nm to 70-80 nm (Table I). Therefore the ring height was increased to more than 80 nm, and the ring outer diameter was increased to about 600 nm. After another 5 min of immersion in the gold electroless solution the gold granule size did not increase, but the ring was filled by more gold particles. If more 5 min immersion steps were employed, the gold ring continued to slightly increase in height, until a total of 4 times (20 min) or immersion, at which the height reached about 150 nm. Meanwhile the inner diameter and outer diameter of the rings were stabilized at 120-180 nm and ~600 nm, respectively. However, when a 20 min immersion step was added after a total of 6 times (30 min) of step-by-step immersion of substrate, large (~110 nm) gold particles was deposited on the initial rings. This could be due to the self-reducing of gold particles from the gold electroless plating solution.

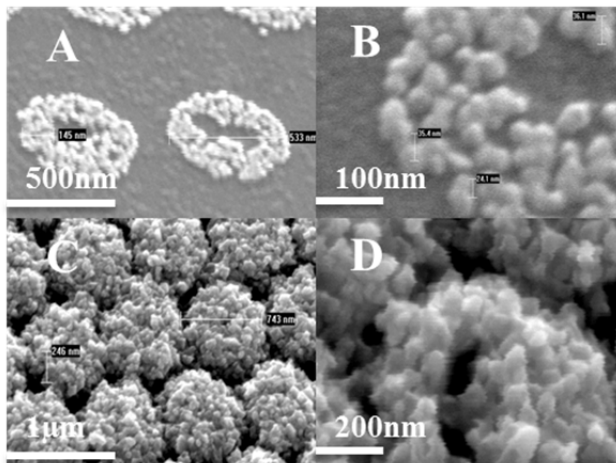


Figure III. SEM images show the original 2D gold nano rings and the continuous 30 min grown hollow gold nanostructures. A. 2D gold nano rings with 500-550 nm outer diameter and 150-200 nm inner diameter; B. Enlarged image for the 2D gold nano rings; C. Hexagonal close packed gold hollow structure with 750 nm in size; D. Enlarged image for the gold hollow structure.

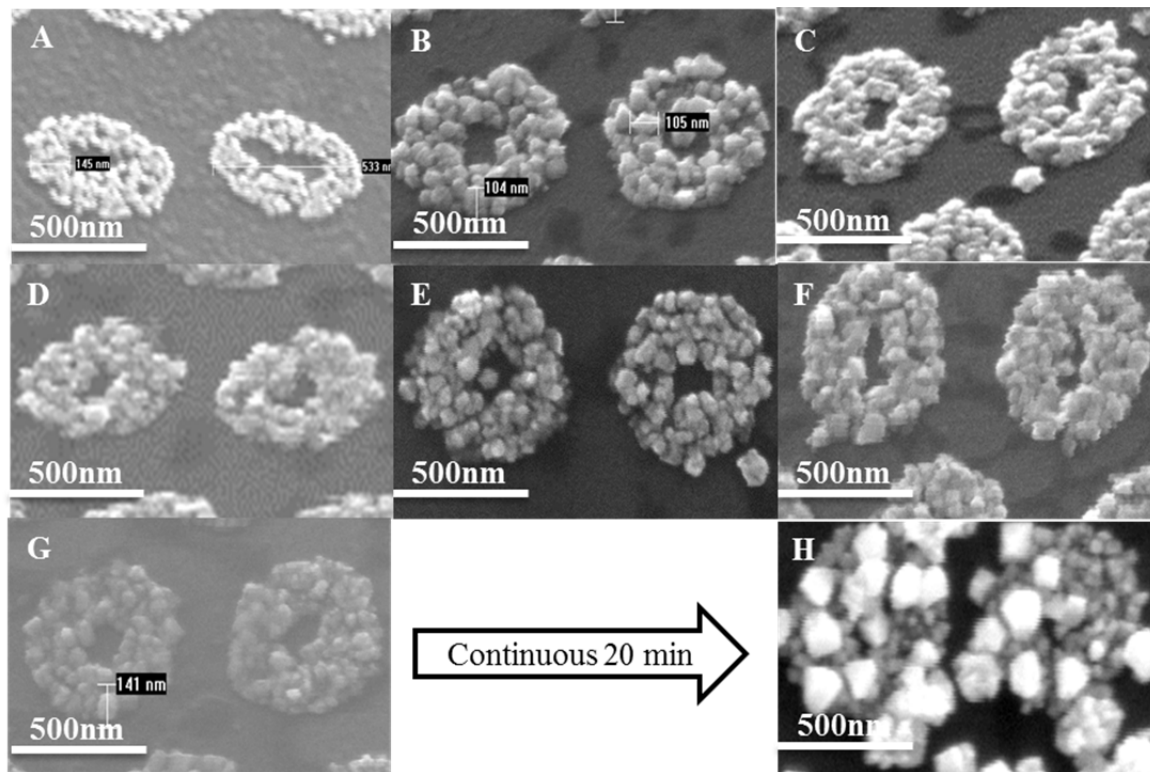


Figure IV. SEM images show step-by-step time dependent growth of the gold nano ring 3D structure based the original 2D gold rings. A. The original gold nano rings; B. The structure in A was grown for 5 min in a gold electroless plating solution; C. The structure in B was grown for 5 min in a gold electroless plating solution; D. The structure in C was grown for 5 min in a gold electroless plating solution; E. The structure in D was grown for 5 min in a gold electroless plating solution; F. The structure in E was grown for 5 min in a gold electroless plating solution; G. The structure in F was grown for 5 min in a gold electroless plating solution; H. The structure in G was grown for 20 min in a gold electroless plating solution.

Table I. The gold nano rings' morphology changes with growing time.

	Growing condition	Inner diameter (nm)	Outer diameter (nm)	Granule size (nm)	Height (nm)
A	Initial rings	~200	~550	20-30	~30
B	5 min from A	~200	~600	70-80	80-100

C	5 min from B	100-200	~600	70-80	100-120
D	5 min from C	120-190	~600	~80	100-130
E	5 min from D	120-180	~600	~80	120-150
F	5 min from E	120-180	~600	~80	130-160
G	5 min from F	120-180	~600	~80	130-160
H	20 min from G	120-180	600-700	~80 and ~110 new particles	210-260 (the new particle height added)
Continuous 30 min growing from A		Closed or ~200 hollow	~750	80-200	250-300

UV-vis spectra and light to heat conversion study of the 3D gold structures. Figure V and VI shows the UV-vis spectra (between 300 and 900 nm wavelength) of five different gold structures (in Figure IV. or Table I. step A, C, E, H and continuous 30 min growing from A). The initial gold nano ring (step A) showed low extinction and the maximum extinction was at ~700 nm wavelength. When rings were immersed for 10 and 20 min (by 5 min step, C and E steps), the extinction increased over the entire wavelength range and two maximum extinction wavelengths (~500 and ~700 nm) were observed. When a 20 min immersing jump was introduced (step H), the extinction was increase from ~0.5 to ~1.0 over the entire wavelength. Meanwhile, the extinction peak at ~700 nm was not observable. The extinction of the continuous 30 min growing substrate showed above 2.0 on the entire wavelength because the gold hollow structure blocked more light than the gold nano rings.

Figure VII shows the transmission of the light through the gold hollow structure was less than 10% at green laser (532 nm), which confirmed the high extinction of the 3D gold hollow structure after continuous 30 min growing. The attenuation, reflection and transmission results measure at 532 nm (green laser) in other growing stages were compared in Figure VII (in Figure IV step C, E, H and continuous 30 min growing). The reflections in the four steps were similar at around 5%, while the transmissions were varied at different steps. The 10 min (step C) and 20 min (step D) 3D gold cylinder like structure showed similar reflection at about 40%, which was higher than the 50 min (step H with large particle deposited on the gold rings) at about 20% and much higher than the continuous 30 min growing gold structure (hollow structure ~750 nm in size) at about 10%.

The hollow gold nanostructures had potential usage as a light harvest material. The thermal response of the different gold nanostructures on ITO glass substrate was studied by using a green laser heating the substrate and a thermal camera recording the temperature change on the substrate. Figure VIII, A shows the power input on the substrates and the maximum temperature increase on the substrates with different gold structures on the substrates. Figure VIII B. shows the light power put into the substrate and the light power come out of the substrate with different gold structures on the substrates. The 30 min continuous grow hollow gold nanostructure had the minimum light power output (at 100 mW input the output was ~5 mW, while the step A and C were at about 40 and 30 mW), because the light was captured by the gold. However, the maximum temperature measured on the substrate was not higher than the other two substrates. The temperatures were all at around 40 °C when 100 mW laser power was applied. A 200 °C/W light to heat conversion was not high compared with reported results [19]. The reason could be although more heat was generated on the hollow gold nanostructure, the good thermal

conductivity of the ITO glass (>0.8 W/mK) compared with the PDMS substrates (0.15 W/mK), the heat dissipated much faster on the ITO glass. The heat dissipation from the gold to the substrates was reported at 100 ps due to the high thermal conductivity of the gold (110 W/mK) [22].

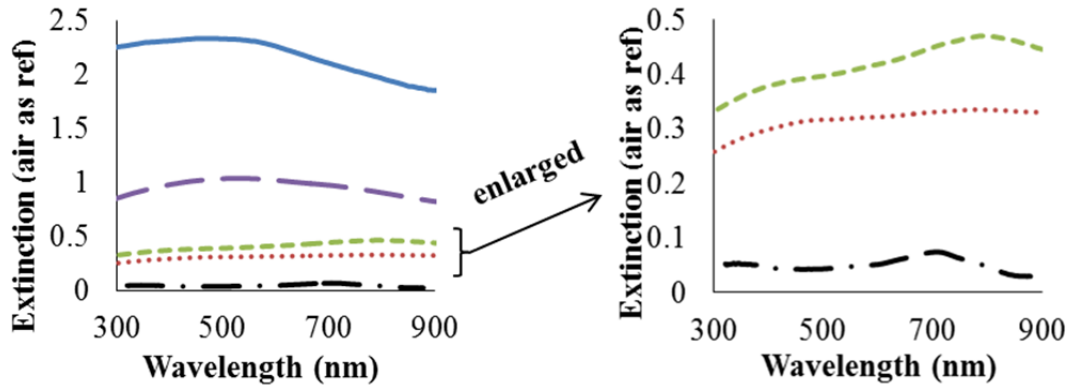


Figure V. UV-vis spectra of the substrates under different growing conditions are plotted (air was set as reference). Black “— . —” represents the original 2D gold nano rings Figure II A; Red “.....” represents the 10 min grown structure Figure IV C; Green “- - -” represents the 20 min grown structure Figure IV E; Purple “- - -” represents the total 50 min grown structure Figure IV H; Blue “—” represents the continuous 30 min growing structure Figure III C and D.

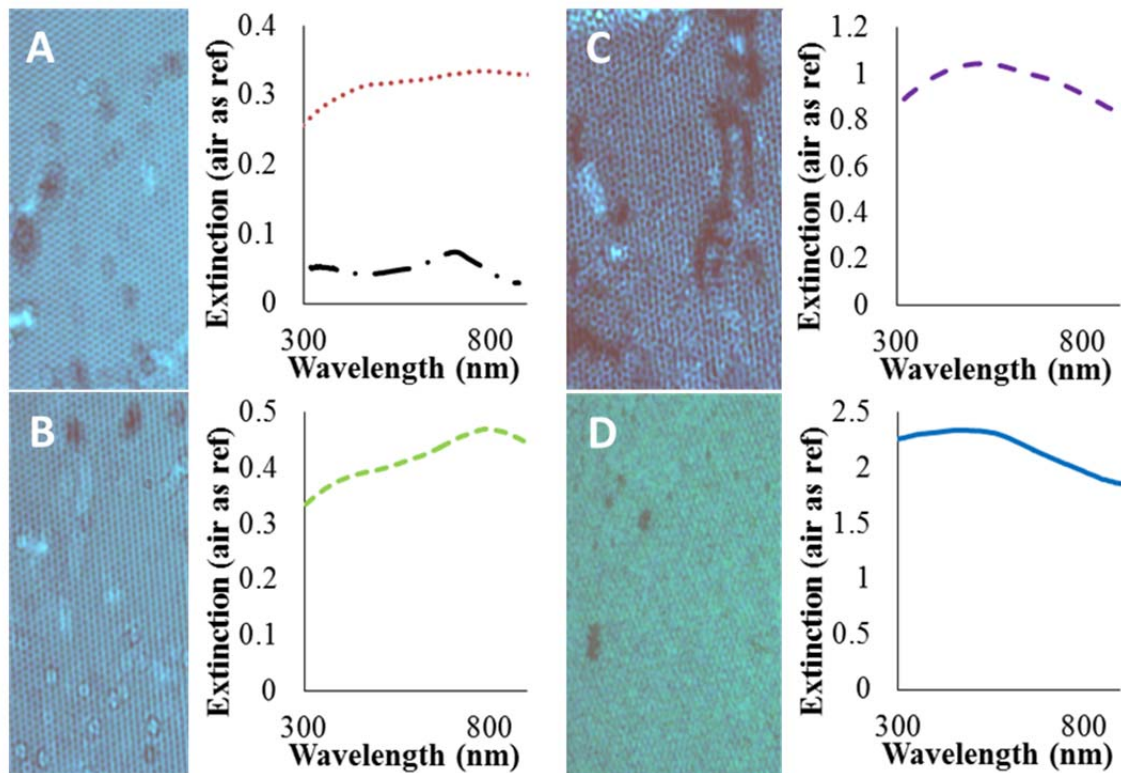


Figure VI. Microscope images of the areas that the UV-vis spectra were taken. A. Red “.....” represents the 10 min grown structure Figure IV C; B. Green “- - -” represents the 20 min grown structure Figure IV E; C. Purple “- - -” represents the total 50 min grown structure Figure IV H; D. Blue “—” represents the continuous 30 min growing structure Figure III C and D.

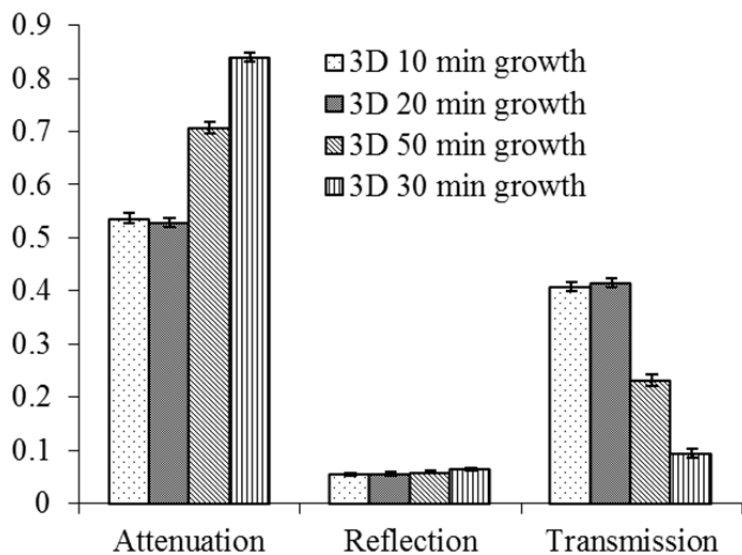


Figure VII. Plot of attenuation, reflection and transmission of the substrates with different structures (Measured by green laser 532 nm irradiation). Pattern “.” represents 10 min grown

structure Figure IV C; Pattern “■” represents the 20 min grown structure Figure IV E; Pattern “▨” represents the total 50 min grown structure Figure IV H; Pattern “|||||” represents the continuous 30 min growing structure Figure III C and D.

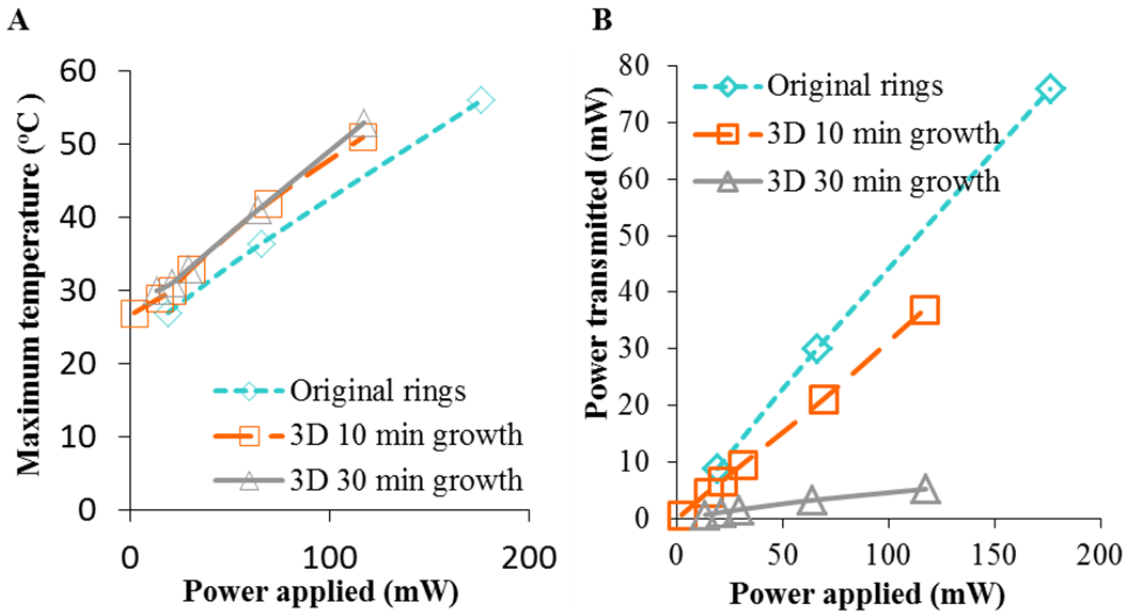


Figure VIII. Thermal response of the substrates under different structures (heated by green laser irradiation at different power output) were plotted in A and B. A. The maximum temperature measured on the substrates under different laser power irradiation; B. Different power output measured after the light penetrated though the substrates under different laser power sources.

D. CONCLUSIONS

Two different nanostructures (2D gold nano ring on indium tin oxide (ITO) substrate and gold thin film with hexagonal arrays of gold nanostructures attached to a scotch tape) were fabricated by a new method, which coupled electron beam lithography and electroless plating. The top gold layer on the scotch tape with hexagonal gold nanostructure arrays showed extraordinary light to heat conversion ($1267\text{ }^{\circ}\text{C}/\text{W}$) compared with gold nano composite PDMS membranes ($720\text{ }^{\circ}\text{C}/\text{W}$) [18. 19]. The 3D gold nanostructures (hollow gold structures, cylinder-like structures, and large gold particles deposited on cylinders) were grown based on the 2D gold nano rings. A continuous 30 min growth method resulted in a hollow gold structure, while a 5

min step-by-step growth method fabricated a gold cylinder-like structure that stopped growing after 20 min. However, if the gold cylinder was again continuously grown for 20 min, large gold particles were deposited on the cylinder. UV-vis spectra showed the hollow gold structure had an extinction of ~ 2.0 at the entire wavelength, the gold cylinder-like structure had extinction between 0.5 and 1.0 at the entire wavelength and the extinction increased when the growing time increased; the initial gold nano rings had extinction less than 0.1 over the entire wavelength. Attenuation, reflection and transmission measurements of the substrates showed the gold hollow structure had the maximum attenuation. However, the temperature increase on the substrate with hollow gold structures was not higher than the other substrates (only 2D gold nano rings and gold cylinder-like structures). The reason was proposed that as the ITO glass substrate had high thermal conductivity, the heat generated dissipated faster than the PDMS substrates. In all, a low reflectivity ($\sim 5\%$) material with ordered arrays of gold nanostructures (based on hexagonal gold nano rings) was fabricated. By tuning the growing method and time on the 2D gold nano rings, the attenuation could be increased from 50% to 85%, which has potential usage in solar cells and sensors [23, 24].

E. REFERENCES

- (1). Aizpurua, J.; Hanarp, P.; Sutherland, D. S.; Kall, M.; Bryant, G. W.; Garcia de Abajo, F. J. *Phys. Rev. Lett.*, 2003, 90, 057401.
- (2). Babayan, Y.; McMahon, J. M.; Li, S.; Gray, S. K.; Schatz, G. C.; Odom, T. W. *ACS Nano.*, 2009, 3, 615-620.
- (3). Banaee, M. G.; Crozier, K. B. *Opt. Lett.*, 2010, 35, 760-762.
- (4). Barchiesi, D.; Kessentini, S.; Guillot, N.; de la Chapelle, M. L.; Grosjes, T. *Opt. Express.*, 2013, 21, 2245-2262.
- (5). Liu, H.; Zhang, X.; Zhai, T. *Opt. Express.*, 2013, 21, 15314-15322.
- (6). McLellan, J. M.; Geissler, M.; Xia, Y. *J. Am. Chem. Soc.*, 2004, 126, 10830-10831.

- (7). Nordlander, P. *ACS Nano* 2009, 3, 488-492.
- (8). Yu, Q.; Guan, P.; Qin, D.; Golden, G.; Wallace, P. M. *Nano Lett.* 2008, 8, 1923-1928.
- (9). Prikulis, J., Hanarp, P., Olofsson, L., Sutherland, D., & Käll, M. *Nano Letters.*, 2004, 4(6), 1003-1007.
- (10). Yan, F., & Goedel, W. A. *Nano Letters.*, 2004, 4(7), 1193-1196.
- (11). Song, Y. M., Jang, S. J., Yu, J. S., & Lee, Y. T. *Small.*, 2010, 6(9), 984-987.
- (12). Leem, J. W., Joo, D. H., & Yu, J. S. *Solar Energy Materials and Solar Cells.*, 2011, 95(8), 2221-2227.
- (13). Akimov, Y. A., & Koh, W. S. *Plasmonics.*, 2011, 6(1), 155-161.
- (14). Kitson, S. C., Barnes, W. L., & Sambles, J. R. *Physical review letters.*, 1996, 77, 2670-2673.
- (15). Ahn, W.; Taylor, B.; Dall'Asen A. G. and Roper, D. K. *Langmuir.*, 2008, **24**, 8.
- (16). Blake, P.; Ahn, W.; Roper, D. K. *Langmuir*, 2010, 26(3), 1533.
- (17). Forcherio, G.T. and Roper, D. K. *Appl. Optics* (2013) 52(25) 6417-6427.
- (18). Berry, K. R.; Russell, A. G.; Blake, P. A.; Roper, D. K. *Nanotechnology* 2012, 23, 375703 (11pp).
- (19). Dunklin, J.; Forcherio, G.; Berry, K.; and Roper, D. K. *ACS Appl. Mat. Interf.*, 2013, 5 (17) 8847-8466.
- (20). Russell, A. Plasmonic Pervaporation via Gold Nanoparticle- Functionalized Nanocomposite Membranes, Ph.D. Thesis, University of Arkansas, 2012.
- (21). Jang, G. G.; Hawkrigde, M. E.; Roper, D. K. *J. Mater. Chem.*, 2012, 22, 21942-21953.
- (22). Jain, P. K.; Lee, K. S.; El-Sayed, I. H.; El-Sayed, M. A. *J Phys Chem B.*, 2006, 110:7238-7248.
- (23). Han, K. S., Shin, J. H., Yoon, W. Y., & Lee, H. *Solar Energy Materials and Solar Cells.*, 2011, 95(1), 288-291.
- (24). Chen, J. Y., Chang, W. L., Huang, C. K., & Sun, K. W. *Optics Express.*, 2011, 19(15), 14411-14419.

VI. CONCLUSION

In this master's thesis we first reviewed the tin sensitization process and the electroless plating method. The addition of stannic chloride solution in the tin sensitization step was found the critical for electroless plating. The mechanism of electroless plating was discussed on both the single-step and two-step tin sensitization method. A rapid, straightforward, spectrophotometric method, based on the redox reaction of tin(II) with a mixture of N-bromosuccinimide (NBS) and 3,3',5,5'-tetramethylbenzidine dihydrochloride (TMB-d) was developed for determining low concentrations of tin(II). The spectral absorption at 452 nm was linear with respect to tin(II) concentration between 0.049 $\mu\text{g/ml}$ and 0.340 $\mu\text{g/ml}$, and the limit of detection (LOD) was calculated (3σ) at 0.013 $\mu\text{g/ml}$. Applying the spectrophotometric method for quantitative measurement of stannous (tin(II)) concentrations, the tin(II) concentration was determined on ceramic substrates. The most important conditions that could affect the tin(II) concentration were different substrates and exposure in air. Tin(II) reagent concentration, sensitization time, and substrate surface area were found not affect the results. 2D hexagonal arrays of gold nano rings were fabricated by coupling EBL and electroless plating. The optical and thermal (green laser heating the substrate) properties were studied for the lifted off gold film with hexagonal gold nanostructures on the scotch tape. The 3D gold nano rings and hollow structures were grown based on the 2D gold nano rings. The dynamics of the growing was discussed and the particle sizes changing with growing time were recorded. Potential usage of such gold nanostructures could be in sensors (SERS), solar cell and light to heat conversion devices.

VII. FUTURE WORK

Applying aged SnCl_4 solution in the tin sensitization step was found to enhance tin sensitization and improve electroless plating. Therefore, aging SnCl_4 and applying the aged SnCl_4 solution would be used in the tin sensitization process. The tin(II) concentration was supposed to increase as the aged SnCl_4 solution was applied. Increased acid concentration was also found to improve particle density and decrease particle size. By improving the tin sensitization process, the final goal is to fabricate a monolayer of tin(II) deposition on the substrate. A monolayer of tin(II) deposition was proposed to be a premier condition for producing uniform metal thin films, which should be comparable to the vapor deposition method.

Selectively oxidizing tin(II) that has uniformly deposited on the substrates would make the electroless plating metallization selective. Water protecting tin(II) from oxidation provides a new idea for selective oxidation of tin(II), other than UV light oxidation tin(II). Keeping the water droplet on the selected part of the substrate, while removing the water at the other parts and exposing the substrates in air, would oxidize the rest of the tin(II) to tin(IV) except for the position that is water-droplet protected. Succeeding processes of silver or palladium activation and electroless metallization could selectively metallize the substrates. Novel ways of keeping water droplets/residues on the substrates in nano scales, such as using glass beads, could lead to a breakthrough technology in fabricating metal patterns.